Master Thesis

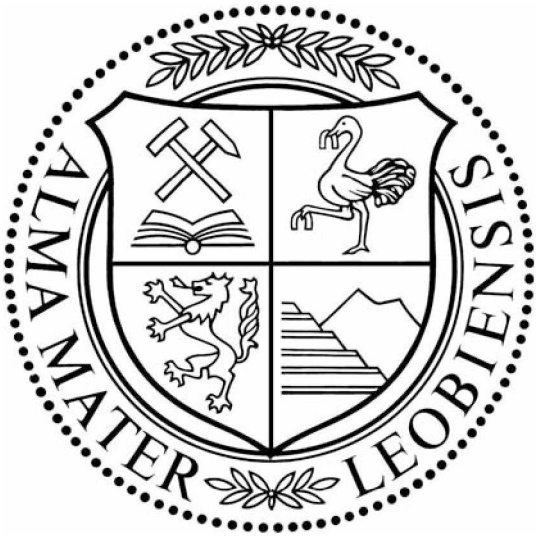

Numerical Modelling of the 2-D Displacement Process Using Polymers

Matthias Buchebner
2011

Department Mineral Resources & Petroleum Engineering
Chair of Reservoir Engineering

Advisor: Univ.-Prof. Dipl.-Geol. Dr. Stephan Matthaei

EIDESSTATTLICHE ERKLÄRUNG

Ich erkläre an Eides statt, dass ich diese Arbeit selbständig verfasst, andere als die angegebenen Quellen und Hilfsmittel nicht benutzt und mich auch sonst keiner unerlaubten Hilfsmittel bedient habe.

AFFIDAVIT

I declare in lieu of oath, that I wrote this thesis and performed the associated research myself, using only literature cited in this volume.

Datum	Unterschrift

I dedicate this work to my parents and to my wife Nasrin Golzadeh, who made this possible. Thanks for the support.

Acknowledgments

I would like to thank Professor Matthaei for his support, that he introduced me to CSMP and the great developer community associated with it and especially for the very valuable retreats and excursions to Plockton/Scotland, Starigrad/Croatia and Potsdam/Germany.

Special thanks to Professor Ganzer for all the great experiences gained while working with him at HOT Engineering and later at the University. Thanks for the support, the great courses and that you enthused me about Reservoir Engineering.

Zusammenfassung

Nur 25% der ultimativen weltweiten Oelvorkommen sind bis heute gefoerdert worden. Da in Zukunft grosse neue Funde immer unwahrscheinlicher werden, fokussiert sich die Forschung darauf, die bestehenden Oelreserven moeglichst effizient auszufoerdern. Um dieses Ziel zu erreichen, bedient man sich fortschrittlicher Methoden, die unter dem Namen Enhanced Oil Recovery (EOR) bekannt sind. Dazu gehoert auch das Fluten der Lagerstaette mit viskosen Polymerloesungen, um das Mobilitaetsverhaeltnis zu optimieren und somit einen hoeheren Ausbeutungsgrad zu erzielen. Heterogene Lagerstaetten sind gute Kandidaten fuer Polymerflutungen weil deren hohe Permeabilitaetsvariabilitaet zu verfruehtem Wasserdurchbruch und zurueckgelassenem Oel fuehren koennen.

In dieser Arbeit werden die Effekte der chemischen und physikalischen Eigenschaften von Polymeren auf das Verdraengungsmuster untersucht. Der praktische Teil ist eine Simulationsstudie, die mit einem kommerziellen Lagerstaettensimulator durchgefuehrt wurde. Zweidimensionale heterogene Modelle wurden mit HYDRO_GEN, einem Programm zur Generierung von stochastischen Permeabilitaetsfeldern, erzeugt. Mit diesen Modellen wurden Sensitivitaetsanalysen durchgefuehrt und miteinander verglichen: die Unsicherheiten der Realisationen wurden bestimmt, der Einfluss von verschiedenen Viskositaetsverhaeltnissen, Brooks-Corey-Parametern, verschiedenen Gittern, verschiedenen Permeabilitaetseterogeneitaeten und verschiedenen numerischen Loesungsmethoden wurde untersucht.

Die Ergebnisse zeigen, wie verschiedene Simulationskonfigurationen das Auftreten von "viscous fingering" und die Effizienz von Polymerflutungen in heterogenen Lagerstaetten beeinflussen und wie geologische Unsicherheiten und Permeabilitaetsheterogeneitaeten sowie die ausgewaehlte numerische Methode Einfluss auf die Simulation von Polymerfluten nehmen.

Abstract

Only about 25% of the ultimate oil resources world wide have been produced so far. Since the chances of discovering new giant fields are getting lower and lower, current research focuses on improving recovery from already explored reservoirs in the most efficient way possible. To achieve this goal, enhanced oil recovery methods (EOR) are essential. One EOR method is flooding the reservoir with viscous polymer solutions to achieve a favourable mobility ratio thus getting a better sweep. Heterogeneous reservoirs are good candidates for polymer flooding because their high variability in permeability promotes early water breakthrough and bypassed oil.

In this work, the effects of the chemical and physical properties on sweep are investigated. The practical part is a simulation study conducted with a commercial reservoir simulation package. Two-dimensional heterogeneous models have been created with HYDRO_GEN, a program for the generation of spatially distributed fields of permeability. On those models, sensitivity analysis have been performed and compared: Uncertainties of different realizations have been determined, the influence of different viscosity ratios, Brooks-Corey parameters, different meshes, permeability heterogeneities and numerical methods have been studied.

Results establish how different simulation configurations influence the onset of viscous fingering and sweep efficiency in heterogeneous reservoirs and show how geologic uncertainty and permeability heterogeneity as well as the selected numerical method have an influence of polymer flooding simulation.

Contents

List of Tables

List of Figures

1 Introduction

To produce oil from a reservoir, energy hast to be supplied. This energy can come from the reservoir itself (e.g. high pressure), from other natural sources (e.g. gravity) or from outside. The first stage of production is called "Primary Recovery", in which the reservoir fluids are produced naturally with the energy from the reservoir. This stage is typical the shortest. After production declines to a certain level, secondary recovery starts. There are three different processes in secondary recovery:

- Pressure maintenance
- Gas Injection
- Waterflooding

Waterflooding is the most common production method in reservoir engineering.[Green and Willhite, 1998], permitting the recovery of about 30-40% of the oil can be recovered.[Littmann, 1988] After secondary recovery processes stop to be efficient, tertiary recovery may be applied. Tertiary recovery methods involve:

- Polymer flooding
- Chemical flooding
- Thermal recovery processes
- Gas injection
- Bacterial EOR

In some offshore wells secondary and tertiary recovery methods are applied right from the beginning.

Only 25% of the ultimate oil resources of the world have been produced until now[Burri, 2008]. The chances to discover new giant oil fields are getting smaller and smaller. That means, that the emphasis has to be set on producing already explored reservoirs more effectively. It does not make sense to spend billions of dollars on exploration while there are unused reserves. The methods described earlier aim at this goal. The main goal of tertiary recovery is to get stable displacement of the reservoir fluid by the producing fluid and thus increasing the recovery factor in a certain time frame.

Not all fields are suited for all types of EOR methods. For example, faulted reservoirs with highly permeable faults may be unsuited for water flooding since most of the injected water could be going down the faults. Very hot reservoirs won't be suited for polymer flooding because the heat will destroy the polymers. A detailed list of influencing factors can be found in the next chapters.

This work is focused on enhanced oil recovery by polymer flooding. A viscous polymer solution is injected into the reservoir to form a stable displacement of the oil (and sometimes to plug high permeable geological structures). As more and more pore volumes are injected, the polymer concentration is reduced for economical reasons. After the polymer slug has reached a certain volume, it is displaced by water.

The process is illustrated below (figure by United States Department of Energy):

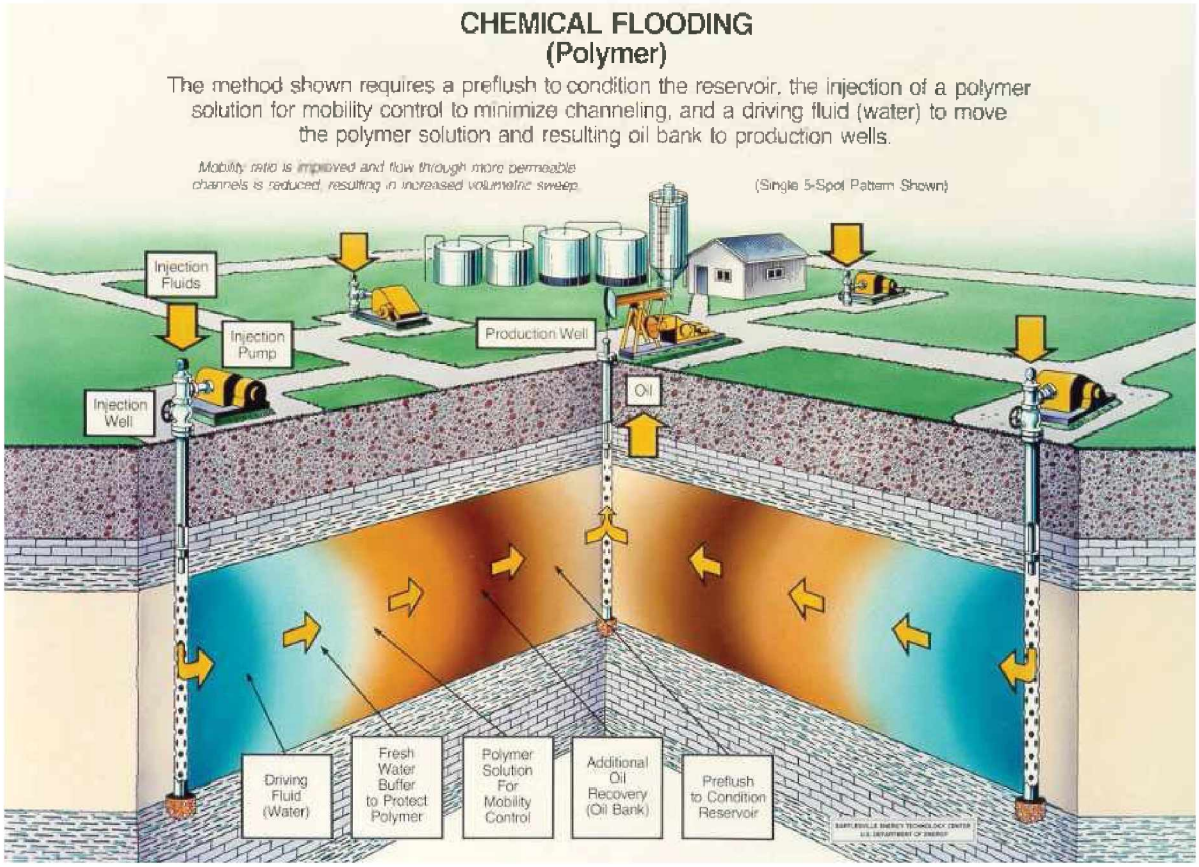

Figure 1.1: Schematic Representation of the Polymer Flooding Process

In a homogeneous reservoir, recovery is expected to be the same for waterflooding and polymer flooding because no interface instabilities are triggered by heterogeneities. However, polymer flooding saves a lot of time. To obtain the same recovery, 10 to 20 times more pore volumes have to be injected in a pure waterflood[Littmann, 1988].

The diagram below[Littmann, 1988] shows the residual oil saturations versus injected pore volumes after polymer flooding has been performed with varying polymer concentrations. It can be seen that higher polymer concentrations lead to a lower residual oil saturation at an earlier time.

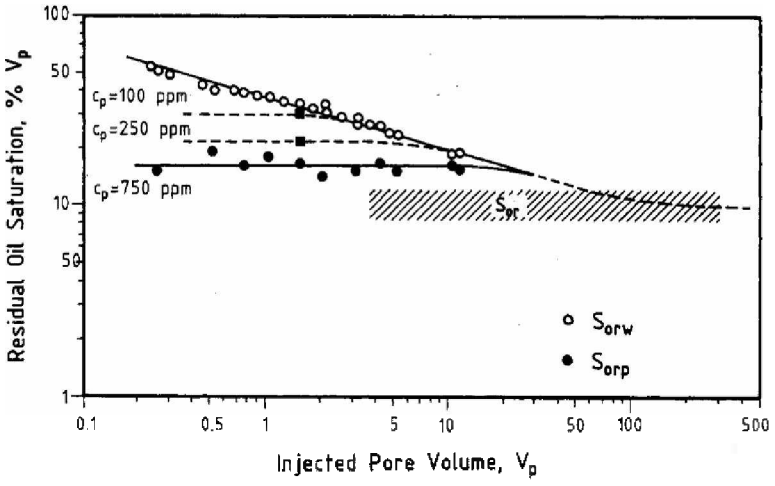

Figure 1.2: Comparison of Water Flooding and Polymer Flooding Effectiveness

Polymer flooding always became interesting when oil prices where high. Research in the field of polymer flooding boomed in the time of oil crisis. Lots of work hast been done in the seventies. When the oil price fell again, research also declined. Since the demand for oil is growing, polymer flooding will be very interesting very soon.

This work has a theoretical and a practical part. In the theoretical part, the physical, chemical and mathematical phenomena of polymer flooding are studied. In the practical part, a two-dimensional simulation study was performed.

1.1 Literature Review

Research on polymer flooding started at the 1960s. After that, a direct correlation of the amount of research and the oil price can be observed since polymer flooding is a rather expensive EOR method.

The most cited publications on numerical simulation of polymer flooding have been published by Bondor et al. and Lutchmansingh. At the present, most of the research is done in China. A review of different approaches to numerical treatment of polymer flooding has been performed and is summarized in table 1.1.

Zeito developed a 3 dimensional, 2-phase, incompressible finite-differences simulator[Zeito, 1968].This simulator cannot model gravitational and capillary forces and dispersion, polymer propagation is modelled by mass transport only. The solution viscosity is a function of polymer concentration.

Graue presented a simple mathematical method to calculate reservoir flooding by a fluid of reduced mobility[Graue, 1968]. The author implemented the method as a computer program, but not as a numerical simulator as calculations are done analytically. He assumed piston-like displacement and his work focused on non-communicating, linear reservoirs.

Patton, Coats and Colegrove used laboratory experiments and an analytical solution to the linear oil displacement process to check the accuracy of their numerical model[Patton et al., 1970]. This model consists of a five-spot finite-difference simulator for multiple layers. The layers are non-communicating. They use the streamtube-approach to model the transport. Polymer/water viscosity is calculated as a function of shear rate and concentration of polymer in the aqueous phase. Adsorption is assumed to be irreversible. Laboratory experiments showed that trailing-edge dispersion had a negligible effect.

Jewett and Schurz developed a two-dimensional five-spot, two-phase finite differences simulator[Jewett and Schurz, 1970]. The layers are non-communicating. They neglected capillary and gravitational forces in their model. Adsorption is modeled as Langmuir-type adsorption (explained later in the thesis)

Slater and Farouq-Ali presented a two-phase, two-dimensional finite-differences simulator[Slater and Farou This model was used by other researchers as a basis for further development.

Bondor, Hirasaki and Tham developed a compressible, three-phase, four-component, finite difference simulator. The polymer solution is modeled as a fourth component of the aqueous phase[Bondor et al., 1972]. Adsorption is calculated as a function of pore volume, adsorptive capacity, polymer concentration and the fraction of the mobile aqueous phase in the grid block. Mobility reduction is modeled as a residual resistance

factor. Non-newtonian rheology is modeled by a modified Blake-Kozeny model for power-law fluids.

Todd and Chase developed a 3 dimensional, finite-difference, incompressible flow simulator called "INTERCOMP"[Todd and Chase, 1979]. It solves for three phase flow and n components, which are able to partition among phases. They incorporated following characteristics of polymer flooding: Inaccessible pore volume, resistance factors, retention hysteresis and dispersion. The recovery mechanisms that can be modelled are swelling, solubilization and interfacial effects.

Bang and Caudle formulated a 3-dimensional, implicit, multi-component, multiphase simulator based on finite differences[Bang and Caudle, 1984]. This model has been verified by history matching of core floods. Their simulator is able to model capillary forces. Physical adsorption is modeled by Fick's law and adsorption is modelled as a Langmuir-type.

Jones et al. developed a predictive method for water/polymer flooding[Jones et al., 1984]. This predictive semi-analytical model has been validated against simulators, field results and analytical calculations. It is not a numerical simulator and yields faster results. Polymer is a dissolved component in the aqueous phase. Inaccessible pore volume is user-defined. The viscosity of the polymer solution is newtonian. Non-Newtonian effects are calculated in the injectivity calculation

Dogru and Yamamoto developed two models[Dogru and Yamamoto, 1984]. Both are capable of 3-D simulation. The first one a limited compositional two-phase, four component simulator, whereas the second one is a fully compositional four-phase, ten-component compositional simulator. The latter is capable of modeling detailed thermodynamic phase relationships, cation exchange, phase trapping, permeability reduction, adsorption/desorption and capillary phenomena.

Bilgesu and Ertekin developed a three dimensional multi-purpose compositional simulator that is able to take capillary pressure effects into account[Bilgesu and Ertekin, 1985]. The rheology of the polymer solution is modeled by a modified Blake-Kozeny model for

power law fluids. Adsorption is modeled as Langmuir-type

Maitin et al. developed "BOSS" ("Black Oil Simulation Software")[Maitin et al., 1988]. BOSS is a 3D-simulator and accounts for three effects occurring because of the presence of polymer in the aqueous phase: Increased viscosity, altered relative permeability as a result of adsorbed polymer and shear rate.

Lutchmansingh describes a three-phase, four component finite-difference simulator in his PhD-thesis[Lutchmansingh, 1987]. Polymer and brine form the aqueous phase. He assumed that the polymer slug cannot be diluted, polymer adsorption only affects aqueous phase viscosity, adsorption is permanent (no desorption), relative permeabilities are only functions of saturation, the viscosity of the polymer solution is independent of the shear rate. Dispersion of the polymer component is modeled with an empirical mixing parameter.

Shiyi et al. developed a three-dimensional. compositional alkali/surfactant/polymer (ASP) flooding simulator[Shiyi et al., 1995]. Capillary pressure and interfacial tension effects are included. It can handle the following transport processes: Convection, diffusion/dispersion, liquid-liquid transfer, liquid-solid transfer, chemical reactions. They also modeled in-situ gelation, viscosity alteration, residual resistance factor, rheology and adsorption.

John et al. implemented a parallel, fully implicit EOS compositional simulator that uses Hand's rule to model the phase behavior of surfactant/oil/brine[John et al., 2005]. Hand's rule is an empirical method to estimate the distribution of a consolute between two phases. The simulation results were validated against UTCHEM (University of Texas). They modeled surfactant phase behavior, interfacial tension, capillary saturation, viscosity alteration, adsorption (Langmuir-type isotherm), relative permeability as a function of trapping number, permeability reduction and inaccessible pore volume.

Verma et al. wrote one of the most recent papers on polymer flood simulation[Verma et al., 2009]. They use Exxon Mobile's EM^{power}simulator, which is able to handle unstructured grids. Both shear-thinning and shear thickening are taken into account. Wellbore transmis-

sibility modification treats the variation of shear rates from the well to the reservoir. Inaccessible pore volume, adsorption, residual resistance factor, polymer degradation, temperature and brine salinity are included in their simulator.

Al Sofi and Blunt used a different simulation approach to simulate polymer flooding: streamline-based simulation[AlSofi and Blunt, 2009]. Their rheological model of non-Newtonian fluids enables the simulator to model the rate-dependent viscosity of the polymer solution accurately. Most other simulators ignore the viscosity-pressure dependence of polymers resulting in too high sweep efficiencies in the simulation studies.

Current commercial reservoir simulators capable of modelling polymer flooding are ECLIPSE by Schlumberger, CMG's IMEX and UTCHEM, developed at the University of Texas. They are all based on the finite-difference method.

All this research, however did not focus on the influence of reservoir heterogeneity and effects of different numerical methods (Finite Difference Method vs. Finite Element/Finite Volume Method) such as grid orientation effects.

Feature	Author / Simulator Name	Zeito	Slater	Patton	Jewett	Bondor	Todd (INTERCOMP)	Bang	Jones	Dogru	Bilgesu	Shiyi	Maitin (BOSS)	Lutchmannsingh	John	Vermon	Al-Sofi	ECLIPSE	UTCHEM	CMG
	Year	1968	1970	1970	1970	1972	1979	1984	1984	1984	1985	1985	1988	1988	2005	2009	2009	current	current	current
2D			X		X						X									
3D		X					X	X		X		X	X				X	X	X	X
Capillary effects		X						X		X	X				X			X	X	X
Adsorption				X	X	X	X	X		X	X	X		X	X	X		X	X	X
Dispersion							X					X		X	X			X	X	X
Inaccessible Pore Volume							X		X						X	X		X	X	X
Rheological effects				X					X		X		X					X	X	X
Two-Phase		X	X							X							X	X	X	X
Three-Phase						X	X							X				X	X	X
Compositional										X		X			X			X	X	X
Chemical Reactions												X						X	X	X
Degradation																X			X	
Temperature Effects																X			X	
Streamline																	X			

Table 1.1: Comparison of Different Simulators

1.2 Claim

In this thesis, I have studied the influence of the polymer flooding parameters viscosity ratio and slug size on various stochastic realizations of two-dimensional models with different permeability heterogeneities. This research has been performed with a commercial finite-difference simulator and the CSP hybrid finite-volume/finite element method[Matthäi et al., 2004].

Since it is not possible to observe viscous fingering due to the limited capabilities of a finite-difference simulator using a five point stencil because of the low number of degrees of freedom of flow directions caused by regular grids, a finite-element/finite-volume based simulator is used to study viscous fingering. The results of both simulators are then compared.

This work is motivated by the fact that treatment of reservoir heterogeneities become

more and more important as the oil resources get lower and lower. Because of the high costs of such methods, numerical simulation hast to be used before applying them. Also, computing technology is getting more and more powerful which makes it possible to use more accurate, but also more complex methods such as the Finite Element/Finite Volume method.

1.3 Agenda

In **Chapter 1**, an introduction to polymer flooding and a literature review is presented.

Chapter 2 presents the methodology of this work. Physics and chemistry of polymers are discussed, the governing equations and methods are presented. Also, the workflow of the simulation studies including the generation of the geological models and their properties is discussed. General insights about the polymer flooding process such as selection criteria etc. is summarized.

Chapter 3 is a presentation of the results of the simulation studies, which are later discussed in **Chapter 4**.

In the **Appendix**, source code of the programs written for this thesis is included.

2 Methodology

Polymer flooding is an enhanced oil recovery process where the main concern is to increase the viscosity of the displacing phase by adding a water soluble polymer to get a favorable mobility ratio. The mobility ratio is defined as following:

$$M = \frac{(\frac{k_{rw}}{\mu_w})_D}{(\frac{k_{ro}}{\mu_o})_d} \tag{2.1}$$

where $k_{rw}$and $k_{ro}$are the relative permeabilities of water and oil, $\mu_w$and $\mu_o$are the viscosities of water and oil. "D" denotes the displacing phase, "d" the displaced phase. The mobility ratio is considered favorable if it is less than one. The main purpose of polymer augmented waterflooding is to develop a uniform sweep pattern. If the mobility ratio is unfavorable, the displacing phase will finger directly to the producing well resulting in early breakthrough.

In practice, a polymer solution consisting of either HPAM (Hydrolyzed Polyacrylamid) or Xanthan is mixed with brine. The concentration of polymer is usually between a few hundred to several hundred ppm and the slug size can be up to 100% PV of the reservoir[Green and Willhite, 1998]. Slugs can vary in composition. First, the highest viscosity slug is injected, first followed by slugs with lower viscosity and finally by brine.

Overall displacement efficiency is defined as the product of macroscopic (or volumetric) and microscopic displacement efficiency.

$$E = E_D E_V \tag{2.2}$$

where E_D, the microscopic displacement efficiency is defined as

$$E_D = \frac{S_{oi} - S_{or}}{S_{oi}} \tag{2.3}$$

EOR processes try to move E_D and E_V towards one. In a typical waterflood example[Green and Willhite, 1
where S_{oi} equals 0.6, S_{or} in the swept region equals 0.35 and macroscopic sweep efficiency is 0.7, the overall displacement efficiency is only 0.35.

Polymer augmented waterflooding affects mostly macroscopic displacement efficiency. Microscopic displacement is not significantly affected by polymer flooding, only if surfactants are added to the phase, e.g. ASP flooding (Alkaline Surfactant Polymer). Reservoir heterogeneity also plays a big role in macroscopic displacement. Figure 2.1[Kaminsky et al., 2007] illustrates different stages of polymer flooding projects.

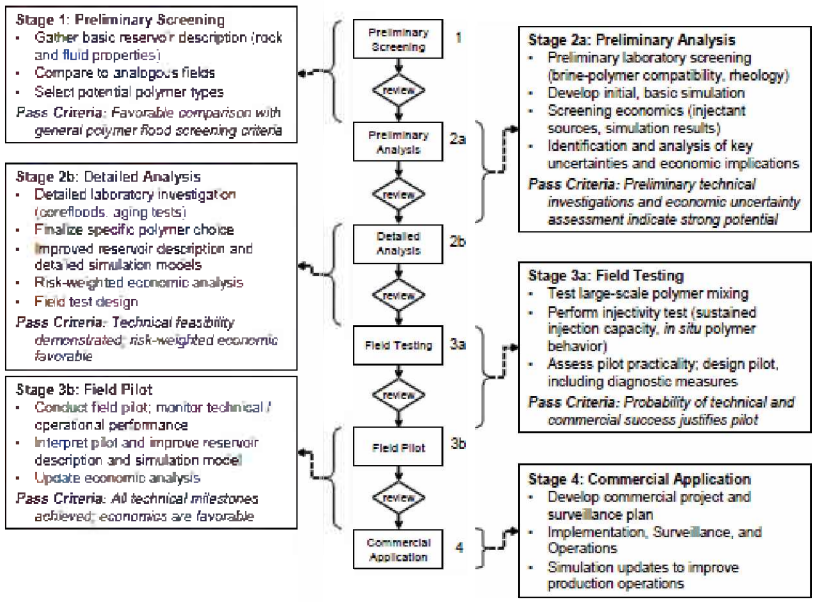

Figure 2.1: Polymer Flooding Explained

2.1 Mathematical Modelling of Displacement Processes

2.1.1 Governing Equations

Reservoir Simulators basically solve two equations numerically, the pressure equation and the transport equation. There are different approaches for solving them. One is the IMPES-approach ("IMplicit pressure, Explicit Saturation"), which aims at solving the the pressure implicitly and therefore in a more stable manner. The saturation is solved explicitly because the saturation gradient is usually smaller than the pressure gradient. Some reservoir simulators solve both equations implicitly. This method is called IMPIMS ("IMplicit Pressure, IMplicit Saturation").

The two-phase slightly compressible pressure equation is defined as[Matthaei, 2008, Chen and Ma, 2006]:

$$c_t \frac{\partial p_t}{\partial t} - \vec{\nabla} \cdot k[\lambda_t \vec{\nabla} p_t + g(\lambda_w \rho_o + \lambda_o \rho_o)\vec{e}_z] - q_t = 0 \tag{2.4}$$

The velocity of the phases are defined as:

$$v_t = k\lambda_t \vec{\nabla} p_r \tag{2.5}$$

$$v_t = v_w + v_o \tag{2.6}$$

$$v_w = \frac{\lambda_w}{\lambda_o} v_o + k\lambda_w \vec{\nabla} p_r \tag{2.7}$$

$$v_o = \frac{1}{1 + \frac{\lambda_w}{\lambda_o}} [v_t - k\lambda_w(\rho_w - \rho_o)g] \tag{2.8}$$

with

$$\overline{\lambda} = \frac{\lambda_w \lambda_o}{\lambda_w + \lambda_o} \tag{2.9}$$

and

$$\lambda_i = \frac{k_{ri}}{\mu_i} \tag{2.10}$$

The IMPES-formulation of the transport equation is:

$$\phi \frac{\partial S_o}{\partial t} + \vec{\nabla} \cdot [v_t f(S_o) - \overline{\lambda}(S_o) k (\rho_w - \rho_o) g_y - \overline{\lambda}(S_o) k \frac{dpc}{dS} \nabla S] - q_o = 0 \tag{2.11}$$

2.1.2 Buckley-Leverett Theory

Buckley and Leverett (1942) were the first ones to develop a model for one-dimensional displacement of oil by water. They made the following restrictive assumptions[Willhite, 1986, Buckley and Leverett, 1942]:

- No mass transfer between phases
- Incompressible flow
- Fractional flow is only a function of the water saturation

In one dimension and conceptualizing flow as the passage through control volumes, the starting point of the derivation of the Buckley-Leverett equation is the law of mass conservations for oil and water:

$$-\frac{\partial}{\partial x}(\rho_o q_o) = A \frac{\partial}{\partial t}(\rho_o S_o \phi) \tag{2.12}$$

$$-\frac{\partial}{\partial x}(\rho_w q_w) = A \frac{\partial}{\partial t}(\rho_w S_w \phi) \tag{2.13}$$

Since we assumed that the flow is incompressible and the porosity is constant, the equations reduce to the following:

$$-\frac{\partial q_o}{\partial x} = A\phi\frac{\partial S_o}{\partial t} \tag{2.14}$$

$$-\frac{\partial q_w}{\partial x} = A\phi\frac{\partial S_w}{\partial t} \tag{2.15}$$

One additional constraint is:

$$S_w + S_o = 1. \tag{2.16}$$

The sum of (2.14) and (2.15) with the boundary condition (2.16) yields

$$\frac{\partial(q_o + q_w)}{\partial x} = 0. \tag{2.17}$$

which means that the total flow is constant. The fractional flow of one phase is defined as the fraction of the total flow.

$$f_o = \frac{q_o}{q_w + q_o} \tag{2.18}$$

and

$$f_w = \frac{q_w}{q_w + q_o}, \tag{2.19}$$

so that

$$f_w + f_o = 1. \tag{2.20}$$

The fractional flow equation is then inserted into (2.15):

$$-\frac{\partial f_w}{\partial x} = \frac{\phi A}{q_t}\frac{\partial S_w}{\partial t} \tag{2.21}$$

$S_w$is a function of x and t.

$$dS_w := \frac{\partial S_w}{\partial x}\,|_t\, dx + \frac{\partial S_w}{\partial t}\,|_x\, dt. \tag{2.22}$$

To solve for a particular saturation S_w, the operator dS_wcan be set to zero. After rearrangement of (2.22) an equation for the velocity of a given saturation $S_w$moving through the porous medium is obtained.

$$\frac{dx}{dt}\,|_{S_w} = \frac{\frac{\partial S_w}{\partial t}\,|_x}{\frac{\partial S_w}{\partial x}\,|\,t} \tag{2.23}$$

Since the fractional flow of water is a function of the water saturation only, and by using the chain rule, (2.24) can be inserted into (2.21):

$$\frac{\partial f_w}{dx}\,|_t = \frac{\partial f_w}{\partial S_w}\,|_t\,\frac{\partial S_w}{\partial x}\,|_t \tag{2.24}$$

(2.24) and (2.23) yield

$$-\frac{\partial f_w}{\partial S_w}\,|_t\,\frac{\partial S_w}{\partial x}\,|_t = -\frac{\phi A}{q_t}\,|_t\,\frac{\partial S_w}{\partial x}\,|_t\,\frac{dx}{dt}\,|\,_{S_w} \tag{2.25}$$

which can be simplified to

$$\frac{dx}{dt}\,|_{S_w} = \frac{q_t}{\phi A}\frac{\partial f_w}{\partial S_w}\,|_t \tag{2.26}$$

This equation is called the "frontal advance equation" or "Buckley-Leverett equation". The solution of this equation is of the following type:

$$S_w(x,t) = S_w(x - V(S)t) \tag{2.27}$$

where

$$V(S) = (\frac{dx}{dt})_{S_w} \tag{2.28}$$

For the graphical construction of the saturation at the front, the so-called fractional flow equation has to be developed. The starting point is the Darcy equation.

$$q_o = -\frac{Ak_o}{\mu_o}(\frac{\partial p_o}{\partial x} + g\rho_o sin\alpha) \tag{2.29}$$

Because $q_w = f_w q_t$ and $q_o = (1 - f_w)q_t$, (2.29) becomes

$$(1 - f_w)q_t = -\frac{Ak_o}{\mu_o}(\frac{\partial p_o}{\partial x} + g\rho_o sin\alpha) \tag{2.30}$$

and

$$f_w q_t = -\frac{Ak_w}{\mu_w}(\frac{\partial p_w}{\partial x} + g\rho_w sin\alpha) \tag{2.31}$$

Rearrangement of these formulas yield:

$$-(1 - f_w)\frac{q_t}{A}\frac{\mu_o}{k_o} = \frac{\partial p_o}{\partial x} + g\rho_o sin\alpha \tag{2.32}$$

and

$$-f_w\frac{q_t}{A}\frac{\mu_w}{k_w} = \frac{\partial p_w}{\partial x} + g\rho_w sin\alpha \tag{2.33}$$

Taking the capillary pressure into account and substraction of (2.33) from (2.32) result in

$$-\frac{q_t}{A}\frac{\mu_o}{k_o} + \frac{q_t}{A}f_w(\frac{\mu_o}{k_o} + \frac{\mu_w}{k_w}) = \frac{\partial P_c}{\partial x} + g(\rho_o - \rho_w)sin\alpha \tag{2.34}$$

This equation is now solved for f_w:

$$f_w = \frac{\frac{\mu_o}{k_o}}{\frac{\mu_o}{k_o} + \frac{\mu_w}{k_w}} + \frac{\frac{A}{q_t}[\frac{\partial P_c}{\partial x} + g(\rho_o - \rho_w)sin\alpha]}{1 + (\frac{k_o}{k_w})(\frac{\mu_w}{\mu_o})} \tag{2.35}$$

If horizontal flow and no capillary pressure effects are assumed, the equation reduces to the following form:

$$f_w = \frac{1}{1 + (\frac{k_o}{k_w})(\frac{\mu_w}{\mu_o})} \tag{2.36}$$

The saturation at the front can be constructed graphically in a $S_w$vs. $f_w$plot by drawing a tangent starting from $f_w = 0$ and $S_w = S_{wc}$to the function. The flood front saturation S_{wf} can be read from the point of tangency as shown in the figure below.

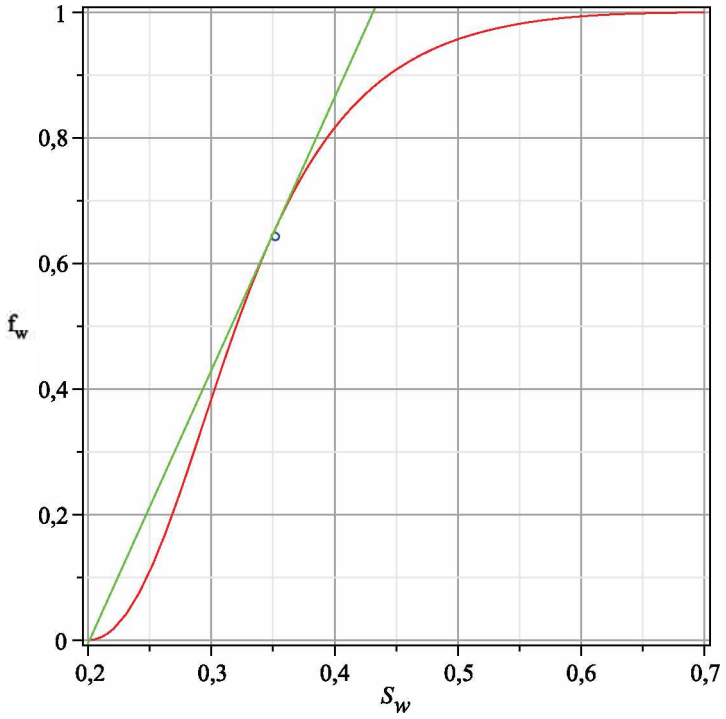

Figure 2.2: Determination of S_{wf}

The next figure illustrates the effect of different viscosities of the displacing fluid. The relative permeabilities are Corey-type permeabilities. The underlying data for the three curves is presented in table 2.1. Corey-type permeabilities are calculated with the

following formulas:

$$S^* = \frac{S_w - S_{wc}}{1 - S_{wc} - S_{or}} \tag{2.37}$$

$$k_{ro} = (1 - S^*)^m \tag{2.38}$$

$$k_{rw} = (S^*)^n \tag{2.39}$$

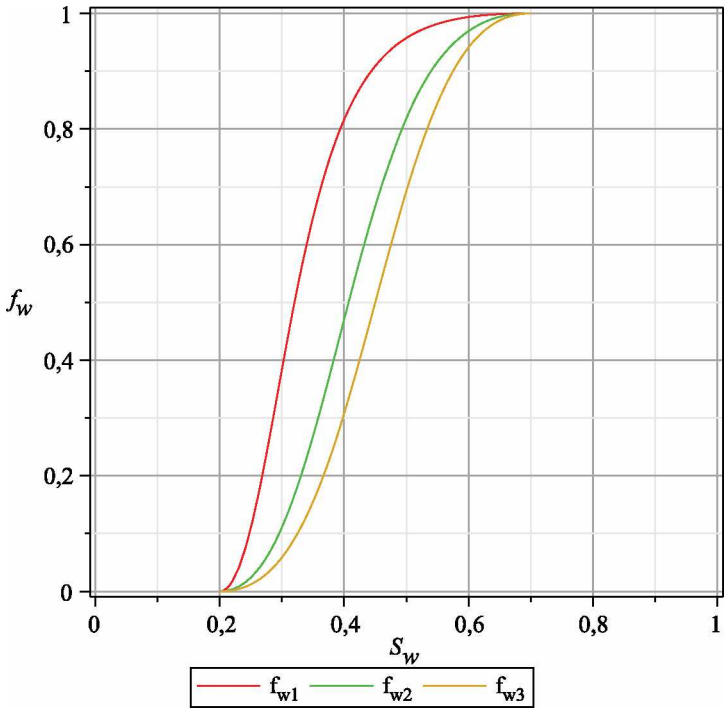

Figure 2.3: Plot of fractional flow curves for different viscosities

m	2
n	2
S_{wc}	0.2
S_{or}	0.3
$\frac{\mu_w}{\mu_o}$ for f_{w1}	0.1
$\frac{\mu_w}{\mu_o}$ for f_{w2}	0.5
$\frac{\mu_w}{\mu_o}$ for f_{w3}	1

Table 2.1: Data for Figure 2.3

Figure 2.3 shows that the higher the viscosity of the displacing phase, the higher the value of $S_w$at the point of tangency (S_{wf}). Thus, $S_w$at the front is higher, oil saturation is lower and this means better efficiency of the flood.

The shape of the saturation function is not continuous. A shock front is developing between the interstitial water saturation $S_{iw}$to the flood front saturation S_{wf}.This is the case because all the saturations lower than S_{wf} travel through the porous medium with the velocity of the flood front. Higher saturations move at a slower speed calculated from equation 2.26.

Figure 2.4 shows the typical Buckley-Leverett saturation profile including the shock and the rarefaction wave.

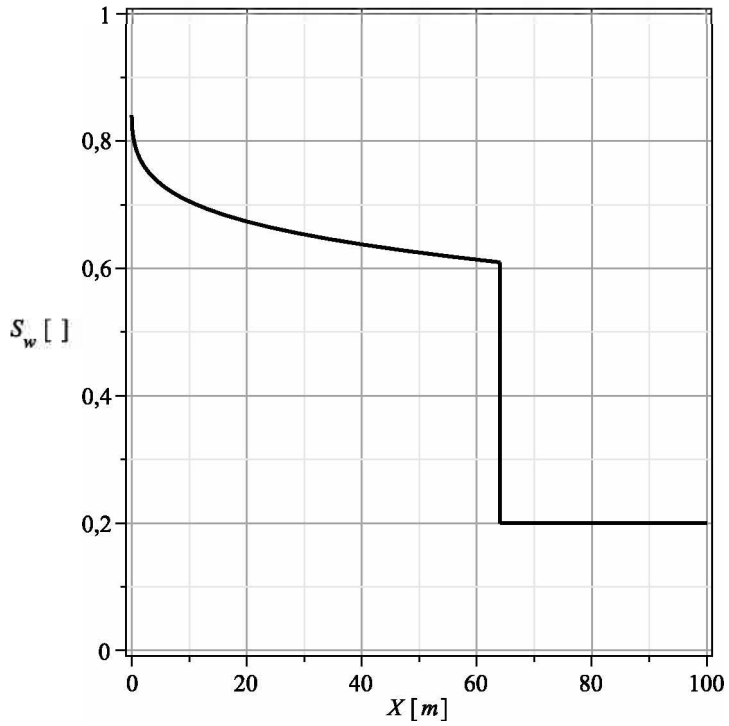

Figure 2.4: Shock front

2.2 Mathematical Background of the CMG Polymer Model / Governing Equations

For this work, IMEX, a part of the CMG reservoir simulation suite, was used. It is a finite-difference three-phase black-oil simulator. Capillary effects and gravity terms are included. The polymer option of IMEX allows the user to model the following phenomena:

- Dispersion
- Adsorption of polymer onto mineral surfaces
- Inaccessible pore volume
- Resistance factor

- Viscosity mixing (linear/nonlinear)

The mass conservation equation for the polymer solution combined with Darcy's law results in the following transport equation:

$$\nabla.(C_p T_w k(\nabla P_w - \gamma_w \nabla h)) + \nabla(\frac{\phi_p S_w D_e}{B_w}).\nabla C_p + q_w C_p = \frac{\partial}{\partial t}(\frac{\phi_p C_p S_w}{B_w} + \phi A_d) \quad (2.40)$$

where C_p the polymer concentration, T_w is the transmissibility for the water phase, P_w is the pressure of the water phase, γ_w is the specific gravity of water, h is the height, ϕ_p is the pore space accessible for the polymer solution, S_w is the water saturation, B_w is the formation volume factor for water, D_e is the effective dispersion coefficient for the polymer component in the water phase, q_w is the water injection rate and A_d is the adsorption/desorption coefficient.

This equation is solved in its finite-difference form:

$$\Delta T_w C_p(\Delta P_w^{n+1} - \gamma_w \Delta D) + \Delta(\frac{\phi_p S_w D_e}{B_w})\Delta C_p^{n+1} + q_w C_p - \frac{V_b}{\Delta t}((\frac{\phi_p S_w C_p}{B_w} + \phi A_d)^{n+1} - (\frac{\phi_p S_w C_p}{B_w} + \phi A_d)^n) = 0 \quad (2.41)$$

where the superscript n+1 means the new time level.

The water transmissibility $T_w$is modified to correctly incorporate the increase of mobility in the water phase due to the presence of polymers.

2.3 Screening of Polymer Flooding Candidates

Reservoir geometry and heterogeneity, reservoir rock, reservoir temperature, permeability, the presence of NaCl play a role in selecting an EOR method. Good candidates for polymer flooding show a bad sweep efficiency in waterfloods, a high watercut, rapid breakthrough and an overall poor performance as compared to similar fields.

		Oil Properties			Reservoir Characteristics					
Detail Table in Ref. 16	EOR Method	Gravity (°API)	Viscosity (cp)	Composition	Oil Saturation (% PV)	Formation Type	Net Thickness (ft)	Average Permeability (md)	Depth (ft)	Temperature (°F)
Gas Injection Methods (Miscible)										
1	Nitrogen and flue gas	> 35 ↗ 48 ↗	< 0.4 ↘ 0.2 ↘	High percent of C_1 to C_7	> 40 ↗ 75 ↗	Sandstone or carbonate	Thin unless dipping	NC	> 6,000	NC
2	Hydrocarbon	> 23 ↗ 41 ↗	< 3 ↘ 0.5 ↘	High percent of C_2 to C_7	> 30 ↗ 80 ↗	Sandstone or carbonate	Thin unless dipping	NC	> 4,000	NC
3	CO_2	> 22 ↗ 36 ↗ [a]	< 10 ↘ 1.5 ↘	High percent of C_5 to C_{12}	> 20 ↗ 55 ↗	Sandstone or carbonate	Wide range	NC	> 2,500 [a]	NC
1–3	Immiscible gases	> 12	< 600	NC	> 35 ↗ 70 ↗	NC	NC if dipping and/or good vertical permeability	NC	> 1,800	NC
(Enhanced) Waterflooding										
4	Micellar/ Polymer, ASP, and Alkaline Flooding	> 20 ↗ 35 ↗	< 35 ↘ 13 ↘	Light, intermediate, some organic acids for alkaline floods	> 35 ↗ 53 ↗	Sandstone preferred	NC	> 10 ↗ 450 ↗	> 9,000 ↘ 3,250	> 200 ↘ 80
5	Polymer Flooding	> 15	< 150, > 10	NC	> 50 ↗ 80 ↗	Sandstone preferred	NC	> 10 ↗ 800 ↗ [b]	< 9,000	> 200 ↘ 140
Thermal/Mechanical										
6	Combustion	> 10 ↗ 16 → ?	< 5,000 ↓ 1,200	Some asphaltic components	> 50 ↗ 72 ↗	High-porosity sand/ sandstone	> 10	> 50 [c]	< 11,500 ↘ 3,500	> 100 ↗ 135
7	Steam	> 8 to 13.5 → ?	< 200,000 ↓ 4,700	NC	> 40 ↗ 66 ↗	High-porosity sand/ sandstone	> 20	> 200 ↗ 2,540 ↗ [d]	< 4,500 ↘ 1,500	NC
—	Surface mining	7 to 11	Zero cold flow	NC	>8 wt% sand	Mineable tar sand	> 10 [a]	NC	> 3:1 overburden to sand ratio	NC

NC = not critical.
Underlined values represent the approximate mean or average for current field projects.
[a] See Table 3 of Ref. 16.
[b] > 3md from some carbonate reservoirs if the intent is to sweep only the fracture system.
[c] Transmissibility > 20 md-ft/cp
[d] Transmissibility > 60 md-ft/cp
[e] See depth.

Table 2.2: Screening criteria for enhanced oil recovery methods

One of the most important factors in polymer flooding is reservoir heterogeneity. Polymer floods stabilize the fronts which are unstable in the presence of high heterogeneity because viscous fingers are triggered.

Taber et al. summarized the screening criteria for EOR methods in a table[Taber et al., 1997].

Littmann presented a guideline based on the following factors: reservoir geometry, reservoir rock, reservoir depth and temperature, crude oil characteristics and reservoir brine characteristics[Littmann, 1988].

2.3.1 Lithology Type

The injectability of polymer solution depends on the mineralogy of the reservoir. Not every rock type is compatible also with every polymer type. The presence of clay may preclude the use of fresh water because of clay swelling. Also, the higher the clay or

carbonate concentration, the higher is the loss of polymer due to adsorption.

Another problem with carbonates is dissolution by fresh water which also makes the water harder potentially changing the properties of the polymer solution. Polyacrylamid polymer viscosity may decrease significantly[Littmann, 1988]. Siliclastic reservoirs are better suited for polymer flooding.

As a rule of thumb found in literature, the porosity should be higher than around 18% and permeability well above 10 mD, otherwise injection pressure is getting too high. It should be between 10 mD and 1 Darcy. At higher permeabilities, waterflooding should be considered because of the higher expenses of polymer flooding operations. Permeability variation also plays an important role. Heterogeneous reservoirs are good candidates for polymer flooding[Carcoana, 1992]. Fractured reservoirs can be treated with crosslinked/gelled polymers which will plug high conductivity zones, preventing early breakthrough[Donaldson et al., 1989].

2.3.2 Reservoir Depth and Temperature

One very important limiting factor in polymer flooding operations is reservoir depth. The injection pressure of polymer solutions is much higher than in normal water injection operations yet it has to be lower than the fracture pressure.

Reservoir temperature also is critical because the behaviour of polymers is very dependent on it. Viscosity of polymer solutions decrease with increasing temperature. Adsorption may also increase. At around 70 ^{o}C, the behaviour of many polymers such as Polyacrylamid changes rapidly[Littmann, 1988].

2.3.3 Crude Oil Characteristics

Polymer flooding is getting more and more useful with increasing gravity of the crude oil because the mobility ratio is getting bigger. If the crude oil is not very viscous, water flooding might be the better (cheaper) method.

2.3.4 Reservoir Brine Characteristics

Reservoir brine characteristics are very important because salinity influence polymer stability. This effect will be described in section 3.3. If salinity is too high, the reservoir has to be preflushed with freshwater. The slug size for this kind of operation is about 0.5 to 1 PV. For lower slug sizes, a preflush with salinity-tolerant polymer can be considered (0.05-0.1 PV)[Littmann, 1988] .

2.4 Chemistry of Polymers

There are basically two kinds of polymers (also called "macromolecules" because of the relatively large size of their molecules) used in polymer flooding: Polyacrylamides, which are artificially created polymers, and polysaccharides, a polymer group created from natural sources.

2.4.1 Polyacrylamides

Polyacrylamides are manufactured by polymerization of acrylamide monomers. A polyacrylamide molecule shows similarity to a flexible coil. Depending on the polymerization process, polyacrylamide molecule weights range from 0.5 million to 30 millions. Polymers used in enhanced oil recovery processes usually have molecular weights ranging from 1 million to ten million, the size of the molecules ranges from 0.1 to 0.3 μm[Littmann, 1988].

The molecules in solution are kept in a straight form because the negative charges of the carboxyl groups repel each other. This causes the molecule to take up the highest possible volume which increases viscosity. This effect can bee seen in figure 2.5[Littmann, 1988]. If cations are present in the water, the molecule curls because the cations compensate the negative charges. This effect lowers the viscosity of the polymer solution. It is also called the "electro-viscous effect". Special polyacrylamides have been developed for more resistance against cations. Normally, polyacrylamides are hydrolyzed from 25-30%. If the degree of hydrolysis approaches zero, the polymer is not as sensitive to

cations[Littmann, 1988].

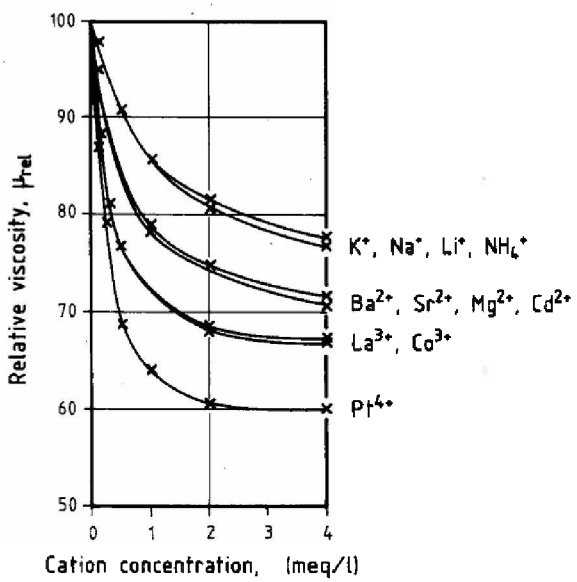

Figure 2.5: Influence of Presence of Cations on Polymer Solution Viscosity

One problem arising is the strong adsorption of polyacrylamide to rock surfaces. To suppress this effect, polyacrylamides are partially hydrolyzed, which means that amide groups (NH_2) are converted into carboxyl groups (COO^-).

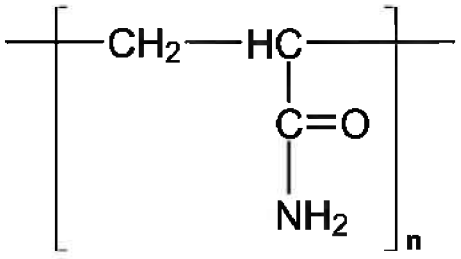

Figure 2.6: Structure of Polyacrylamide

2.4.2 Polysaccharides

Polysaccharides have the general formula $C_x(H_2O)_y$. The variables x and y are usually between 200 and 2500. The most common polysaccharide in use for polymer flooding is

Xanthan, which is produced by fermentation of glucose by the bacterium *Xanthomonas campestris*. Xanthan polymers have molecular weights between 1 million and 15 million.

Xanthan is not as sensitive to salinity as polyacrylamides, however, it is more susceptible to bacterial degradation than artificial polymers. The side changes are also electrically charged, but the molecule is stiffer than the polyacrylamide due to its side chain architecture.

Other polysaccharides produced by microorganisms are Alginate, Curdlan, Scleroglucan, Pullulan and Dextran[Littmann, 1988]. Figure 2.7[Steinbuechel, 2003] shows the structure of Xanthan.

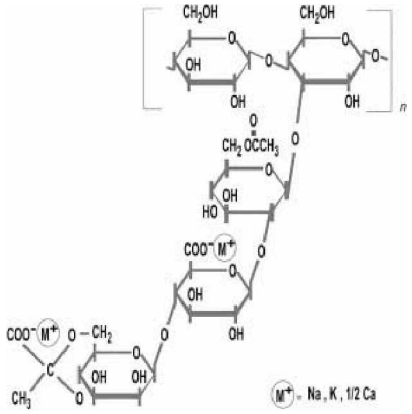

Figure 2.7: Structure of Xanthan

2.5 Physics of Polymer Flooding

2.5.1 Inaccessible Pore Volume

Due to the relatively large polymer molecules, not all of the pore space is accessible to them. Only the aqueous component of the polymer solution may passage the small openings, The pore spaces not contacted by polymer molecules is called "inaccessible pore volume" (IPV). That leads to the effect, that the polymer molecules arrive at the well earlier than it is expected, which is beneficial for economic reasons since oil can be produced earlier. However, this effect also leads to bypassed oil which leads to the

opposite effect.

The effect of polymer adsorption is also reduced because less pore area gets in contact with the polymers. Because the effect of inaccessible pore volume results in the opposite effect (the polymer slug lags behind instead of moving forward relative to the transport medium), polymer breakthrough can be at the same time as tracer breakthrough.

The amount of pore volume not accessible for polymer molecules is defined as ϕ_{IPV}. The constant IPV ranges from 1% up to 30% depending on the polymer and the rock type.[Green and Willhite, 1998] and is assumed to be constant in the field:

$$\phi_{IPV} = (1 - IPV)\phi \tag{2.42}$$

The influence of this factor on recovery and sweep efficiency will be studied in the practical part.

2.5.2 Polymer Retention/Adsorption

Retention of polymers flowing through a porous medium occurs primarily because of two effects:

- Pores that are relatively small in comparison with the polymer molecules block the flow for them
- Polymer molecules adsorb at the wall of the porous medium

Retention is considered irreversible most of the time.[Green and Willhite, 1998] Desorption occurs at a very small scale in comparison with adsorption. However, if flow rates are changed in a large scale after polymer injection at a constant rate in which polymer concentration reached a steady-state condition, "hydrodynamic retention" occurs. If the injection rate is lowered again, polymer molecules are released again and one might observe a higher polymer concentration than it was in the injected fluid.

Adsorption rates usually vary between 20 µg polymer per gram of rock and 700 µg polymer per gram of rock. The lower the degree of hydrolysis, the higher the amount of adsorption. Biopolymers such as Xanthan show lower adsorption values than polyacrylamides. Retention of biopolymers may also be lower if oil is present.[Kolodziej, 1988] Polymer adsorption is also an important screening candidate. A too high adsorption rate results in a high loss of polymer and in consequence, viscosity. However, a certain amount of adsorption is desirable to get a favourable residual resistance factor.

Adsorption of polymers can be modeled using Langmuir isotherms using the following formula:

$$C_{adsorbed} = a_1 \frac{a_1 b_1 C}{1 + b_1 C} \tag{2.43}$$

where C is the concentration and $a_1$and $b_1$are constants. Below is a typical adsorption diagram for $a_1$and $b_1$equal to unity.

At low concentrations adsorption raises rapidly. With increasing concentration, additional adsorption decreases.

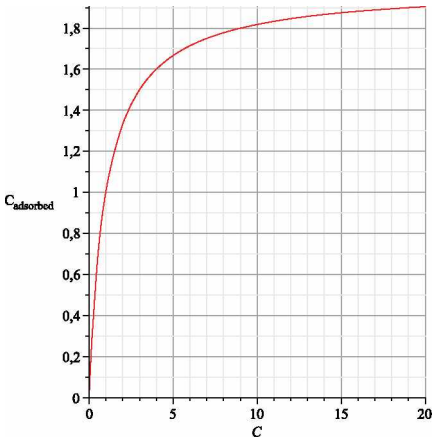

Figure 2.8: Adsorption Isotherm

2.5.3 Viscosity Effects and Resistance Factor

Polymers are used to alter the mobility of the displacing phase. The modified mobility is defined as:

$$\bar{\lambda}_w = \frac{\bar{k}k_{rw}}{\bar{\mu}_w} \tag{2.44}$$

where $\bar{k}$ is the reduced permeability of the rock, caused by adsorption/retention of solid/polymer on the rock face and $\bar{\mu}_w$is the viscosity of the aqueous phase increased by adding polymer to the solution.

The reduced permeability of the reservoir rock, $\bar{k}$, can be expressed empirically using the resistance factor R_w.

$$\bar{k} = \frac{k}{R_w} \tag{2.45}$$

The resistance factor is dependent on the cumulative adsorption, the adsorption capacity of the rock and on the residual resistance factor R_{rf}. They are functions of rock permeability.

$$R_w = 1 + (1 - R_{rf})\frac{A_d}{A_{dmax}} \tag{2.46}$$

There are two methods to calculate the viscosity of the polymer solution. The linear and the nonlinear mixing rule. Empirical tables can also used as well. The linear model is given by:

$$\bar{\mu}_w = \alpha\mu_p^0 + (1 - \alpha)\mu_w \tag{2.47}$$

The parameter α the ratio of the actual polymer concentration, C_p, and the reference polymer concentration, C_p^0.

$$\alpha = \frac{C_p}{C_p^0} \tag{2.48}$$

The nonlinear model is defined as:

$$\bar{\mu}_w = (\mu_p^0)^\alpha + (\mu_w)^{1-\alpha} \tag{2.49}$$

2.5.4 Viscous Fingering

Viscous fingering is an instability in the displacement front that is observed when the displacing fluid forms fractal-like fingers through the displaced phase due to an unfavorable mobility ration. Most of the experimental work on viscous fingering has been performed in so-called Hele-Shaw-cells. A Hele-Shaw cell consists of two parallel glass plates with a small gap. In this gap, A viscous fluid is displaced by a less viscous phase and viscous fingering can be observed. An example of viscous fingering is depicted below (redrawn)[Christie, 1989]:

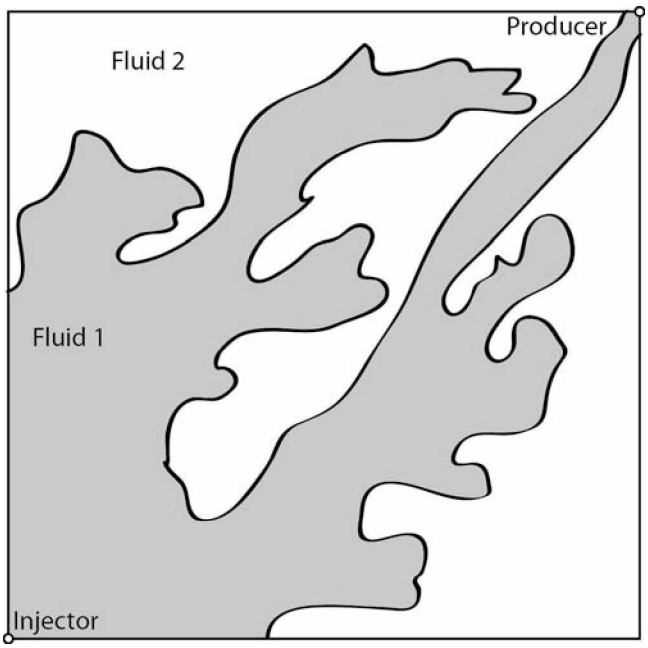

Figure 2.9: Viscous Fingering

The Buckley-Leverett approach to two-phase flow in porous media assumes a stable interface between the displaced phase and the displacing phase and is not applicable for this physical phenomenon. It can however be described by combining Darcy's law with a boundary condition accounting for interfacial tension between the two phases. Viscous fingering occurs at mobility ratios higher than unity which is called "unfavorable" in the literature[Littmann, 1988].

One mathematical model to describe viscous fingering was developed by Collins[Collins, 1961, Willhite, 1986]. A linear, miscible displacement of oil by a solvent is performed in a medium of the length l. The front of the solvent is located at x_f. A perturbation of the solvent front develops at the position $x_f + \epsilon$. If ϵ grows in time, viscous fingering will form If it does not grow, the front remains stable. Darcy law for the two phases and steady-state pressure yields:

$$(\Delta p)_{x_f} + (\Delta p)_{L-x_f} = \frac{u\mu_s x_f}{k} - \frac{u\mu_o(L - x_f)}{k} \tag{2.50}$$

The interstitial front velocity $u(x)$ is defined as:

$$u = \frac{dx_f}{\phi dt} \tag{2.51}$$

The velocity of the front is:

$$\frac{dx_f}{dt} = \frac{-k\Delta p}{\phi\mu_s x_f + \phi\mu_o(L - x_f)} \tag{2.52}$$

The viscosity ration $R = \frac{\mu_o}{\mu_s}$is inserted in the equation:

$$\frac{dx_f}{dt} = \frac{-k\Delta p}{\phi\mu_s[RL + (1 - RL)x_f]} \tag{2.53}$$

The same can be expressed for the region of the perturbation:

$$\frac{d(x_f + \epsilon)}{dt} = \frac{-k\Delta p}{\phi\mu_s[MRL + (1 - RL)(x_f + \epsilon)]} \tag{2.54}$$

Subtracting of the two equations yields:

$$\frac{d\epsilon}{dt} = \frac{k\Delta p(1 - R)\epsilon}{\phi\mu_s[RL + (1 - R)x_f]^2} \tag{2.55}$$

One solution of this ordinary differential equation is:

$$\epsilon = \epsilon_0 e^{Ct} \tag{2.56}$$

$$C = \frac{k\Delta p(1-R)}{\phi\mu_s[RL+(1-R)x_f]^2} \tag{2.57}$$

The variable ϵ_0 is the initial length of the perturbation and depends on the heterogeneity. Because Δp is negative, ϵ will increase exponentially if $R > 1$, if the mobility ratio is smaller than 1, it will decay exponentially leading to a stable flow.

2.6 Geostatistics and Variograms

Spatial properties such as permeability, ore content any other variable that varies in space are not known for every coordinate. Instead, a number of samples are taken. To get a measurement of the spatial variance of such variables, semivariograms (also called "variograms") are used. Variogram analysis assumes the principle of stationarity, that means, the variance of two data points with a certain distance from each other is independent of the position of the datapoints. This principle is illustrated in figure 2.10. Point 1 has the same distance from point 2 as point 3 from point 4. The variance of the spatial property z is the same for the two data pairs.

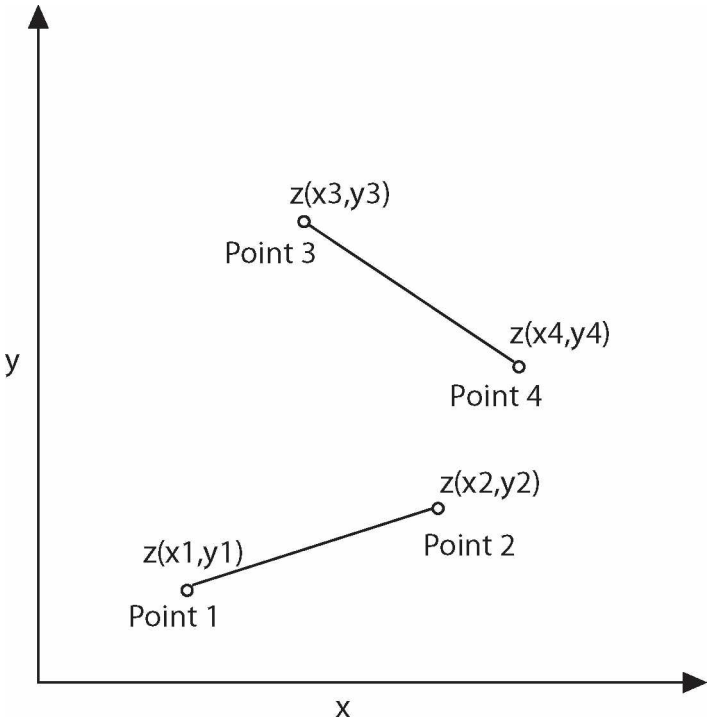

Figure 2.10: Stationarity

A semivariogram plots the variance in respect to the distance. A number of samples are recorded and the distance to each other is calculated. Then, for each sample, the variance to the other samples is calculated. The distance of two data points is called "lag". The variogram is defined as[Cressie, 1993]:

$$2\gamma(h) = \frac{1}{N(h)} \sum (z(x_i, y_i) - z(x_j, y_i))^2 \tag{2.58}$$

$h$is the distance between the two data points $z(x_i, y_i) - z(x_j, y_i)$, $N(h)$is the number of data available for this distance (a tolerance may also be defined). The term $2\gamma(h)$is called variogram and $\gamma(h)$is called semi-variogram.

A semivariogram can be drawn (see figure 2.11) with these data points and different attributes can be read out of it:

- "nugget": Theoretically, two data points with the distance zero should have a vari-

ance of zero. In reality, that's not true due to measurement inaccuracy. It can be seen analogous to the white-noise-effect in signal processing[Wackernagel, 1995].

- "sill": the sill represents the maximum variance. Not all variograms show a sill.
- "range": The distance at which the sill is reached. At greater distances than that, the values do not correlate.

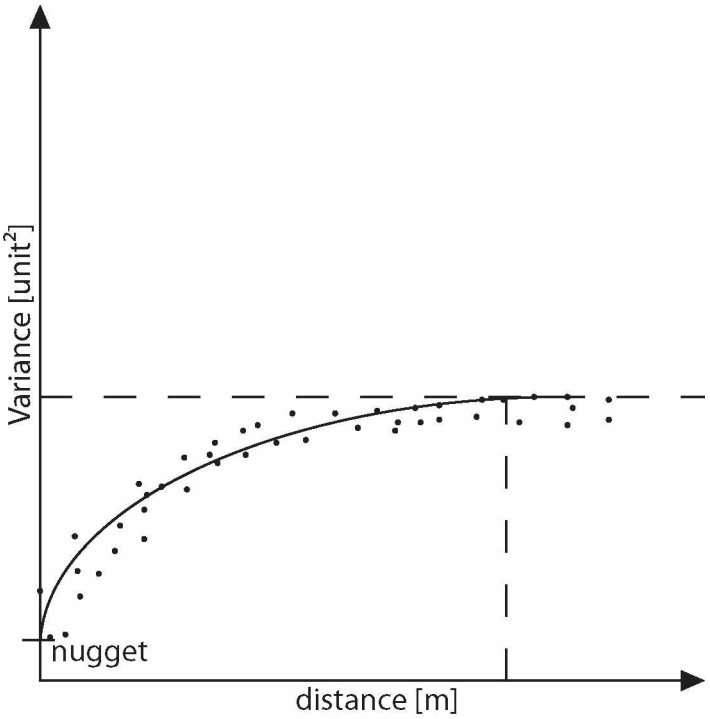

Figure 2.11: Example of a variogram

-

There are different models of V. They include[Wackernagel, 1995]:

- Nugget-effect model
- Gaussian model
- Exponential covariance function

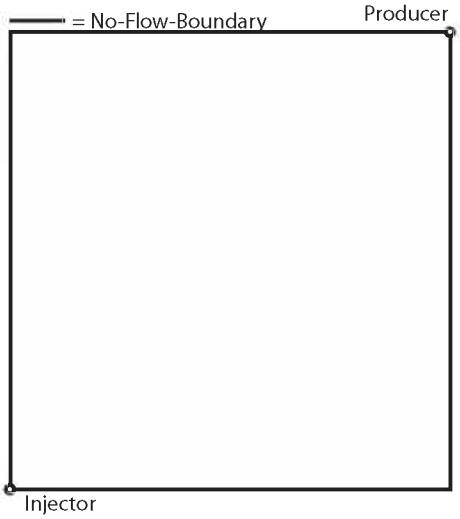

Figure 2.12: Quarter of a five-spot

- Spherical model
- Power-law model (discussed in greater detail in chapter 2.7.1)

2.7 Simulation of Polymer Flooding

2.7.1 Simulation Models

The simulation model used in this study is the widely used quarter-of-a-fivespot pattern. It consists of a square with an injector in the lower left and an producer in the lower right. The field is initially saturated with oil. The injector injects water or a polymer solution with a pressure of 3*10^6 Pa. The producer is producing with atmospheric pressure (100325 Pa). The edges of the square are no-flow boundaries.

2.7.2 Permeability Fields and Permeability/Porosity Correlation

Different stochastic realizations of permeability fields have been created. The open-source software package "HYDRO_GEN" has been used to generate them. The porosity of the cells of the models is calculated through a Kozeny-Karman-type porosity-permeability

correlation. Kozeny-Karman correlations have the form $k = f(\phi^3)$. For this study, the function $k = 9 * 10^4(\phi^3)$ has been chosen, with k in Millidarcies. Normally, porosity is measured and permeability is calculated, in this case it's the other way round, so $\phi = (\frac{k}{9*10^4})^{\frac{1}{3}}$. Porosity values above 47,6% are cut off, since that's the maximum porosity value for cubic packing of perfect spheres.

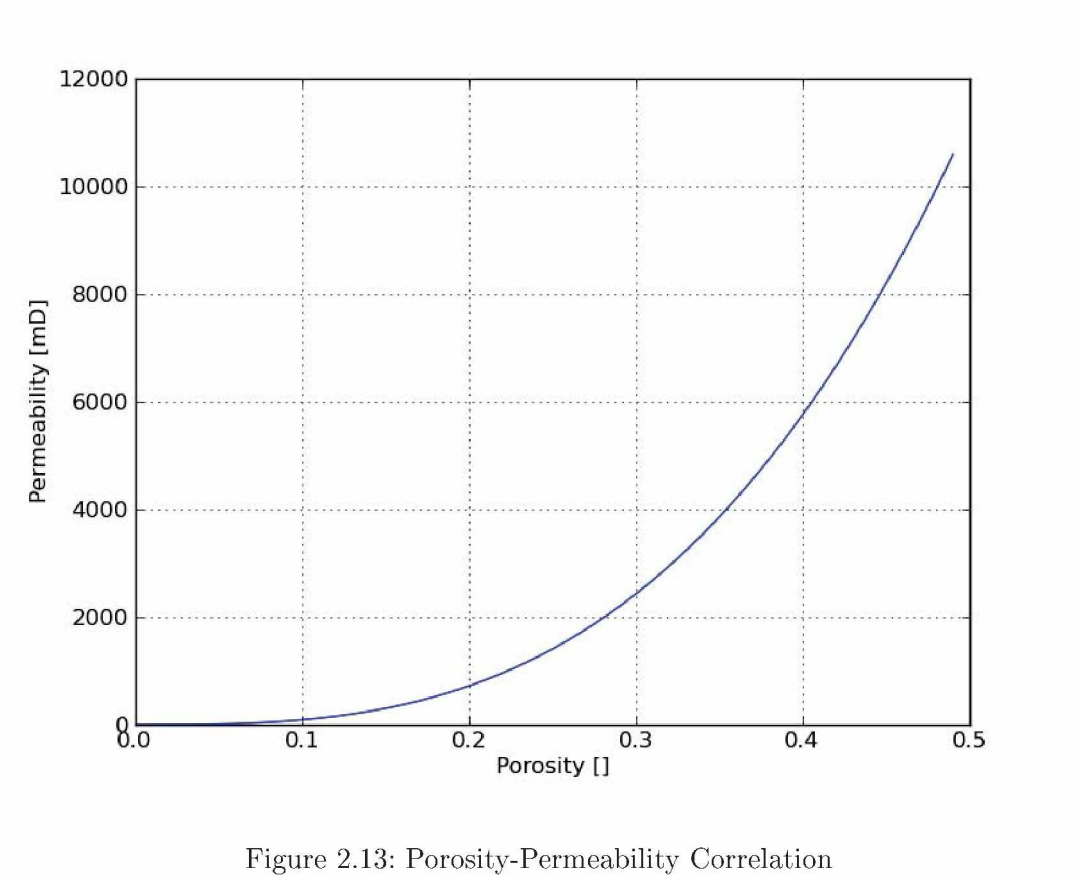

Figure 2.13: Porosity-Permeability Correlation

For the permeability field generation, a power law model has been selected. Power-law models result in self-similar fractal fields. The resulting permeability fields are semivariograms characterized by the power-law equation[Bellin and Rubin, 1996]:

$$\gamma_Z(r) = cr'^{\beta} \tag{2.59}$$

where the constant c is a measure of the variance, β controls the growth of the semio-

variogram with distance, it is related to the Hurst coefficient H:

$$\beta = 2H \tag{2.60}$$

If $\beta < 1$, the resulting picture is grainy and the properties are correlated only over a very short distance. In the opposite case, the result is smooth, but the contrast over large distances is larger. The dimensionless variable r' is the two-points lag, that means the distance between two points in space.

$$r' = \sqrt{r_x^2 + r_y^2} \tag{2.61}$$

$r_x$and $r_y$are the distances between two points in x and y direction.

The dimension of the fractal, also known as "Hausdorff-Dimension" is defined as:

$$d = \frac{ln(\gamma_z(r))}{ln(c)} \tag{2.62}$$

The variance can be visualized using semivariograms or variograms. They show the variance of specific variables in respect to the distance of two points. There are other models than the already explained power-law variogram such as the exponential model, the spherical model and the Gaussian model.

The above picture shows the influence of the exponent. The larger the exponent, the larger the growth of the variance. For smaller values of the exponent, a sill can be identified. For larger exponents, a clear sill cannot be observed. For values above one the variance grows over proportional with the range.

2.7.3 Relative Permeabilities and Capillary Pressure

For relative permeability, a Brooks-Corey-type model was used. It is defined as:

$$S_e = \frac{S_w - S_{rw}}{1 - S_{rw} - S_{rn}} \tag{2.63}$$

$$k_{rw} = S_e^{\frac{2+3\lambda}{\lambda}} \tag{2.64}$$

$$k_{nrw} = (1 - S_e)^2(1 - S_e^{\frac{2+\lambda}{\lambda}}) \tag{2.65}$$

This model has the parameters S_{rw},$S_{rnw}$and λ, which is also called "Brooks-Corey"-parameter. According to Helmig[Helmig, 1997], this parameter ranges from 0.2 to 3.0 and is reverse proportional to the grain uniformity. Figure 2.14 shows relative permeability curves for a Brooks-Corey parameter of 2.5, a residual saturation of the wetting phase of 0.02 and a residual saturation of the non-wetting fluid of 0.2.

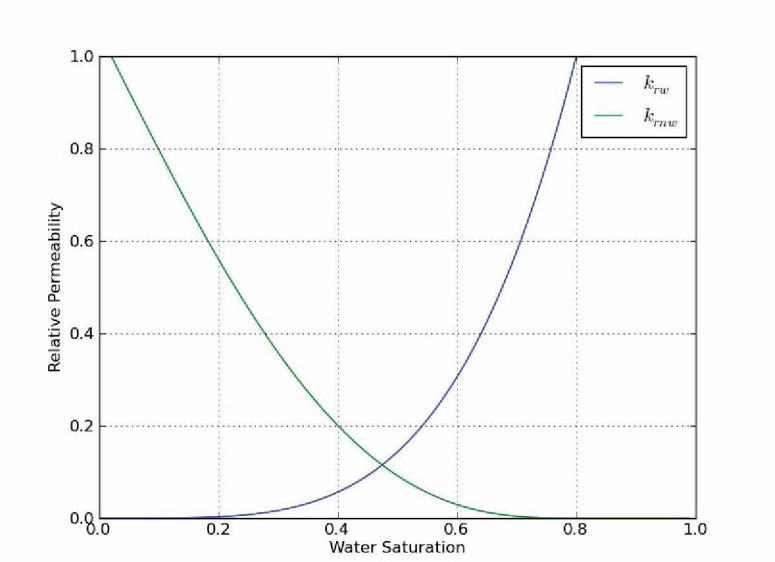

Figure 2.14: Brooks-Corey Relative Permeability Curves

The Brooks-Corey capillary pressure relationship is defined as[Helmig, 1997]:

$$p_c(S_w) = p_d S_e^{-\frac{1}{\lambda}} \tag{2.66}$$

$p_D$is the entry pressure. It is the capillary pressure required for the non-wetting phase to enter the largest pore of the porous medium in case it is filled with the wetting fluid.

Figure 2.15 shows a capillary pressure diagram for the same values as above and an entry pressure of 2*10^5 Pa.

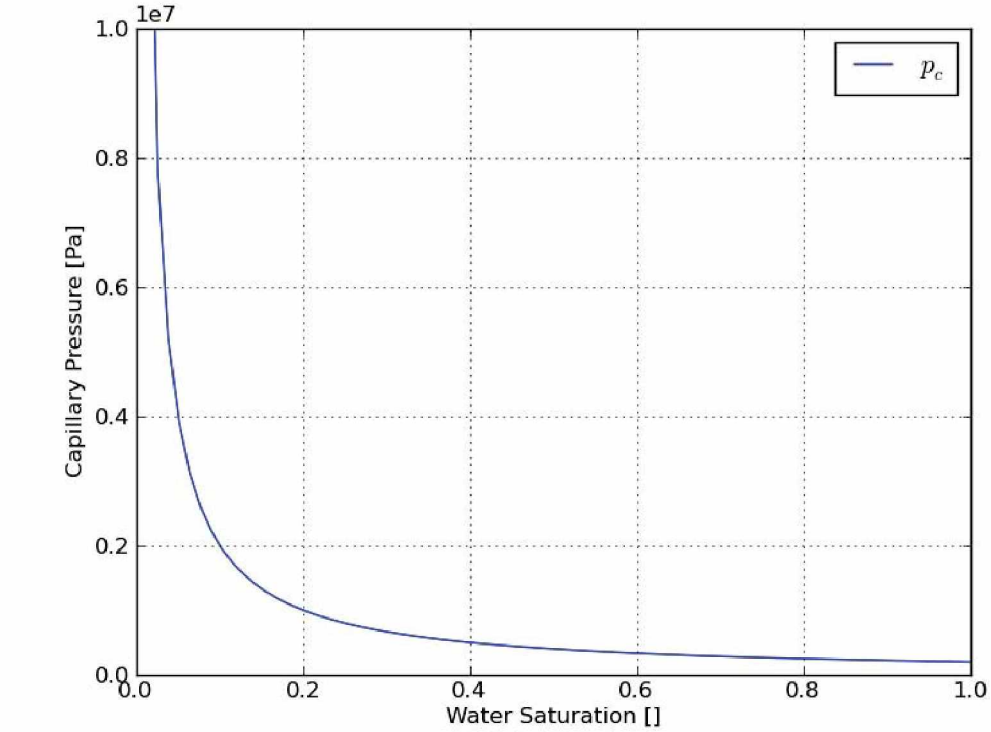

Figure 2.15: Brooks-Corey Capillary Pressure

In CSP, capillary effects are modeled as capillary diffusivity D_c. It is defined as[Helmig, 1997]:

$$D_c = k\lambda_n f_w \frac{dp_c}{dS_w} \tag{2.67}$$

2.7.4 Grid Generation

To study the influence of different grids configurations, python-scripts were written to generate point-clouds that were later meshed using the Triangle-program[Shewchuk, 2005]. This program can be used to triangulize point clouds and generate point clouds automatically. However, the author had to write own python programs to generated the point

clouds because triangle's angle constraints could not be met for equilateral triangles that are needed to get hexagon meshes.

Two types of meshes have been generated to study the effect of different grid configurations due to the different degrees of freedom in each mesh using CSP.

1. Meshes with squares split into two triangles

2. Hexagon meshes

The grids can be seen in figures 2.16 and 2.17.

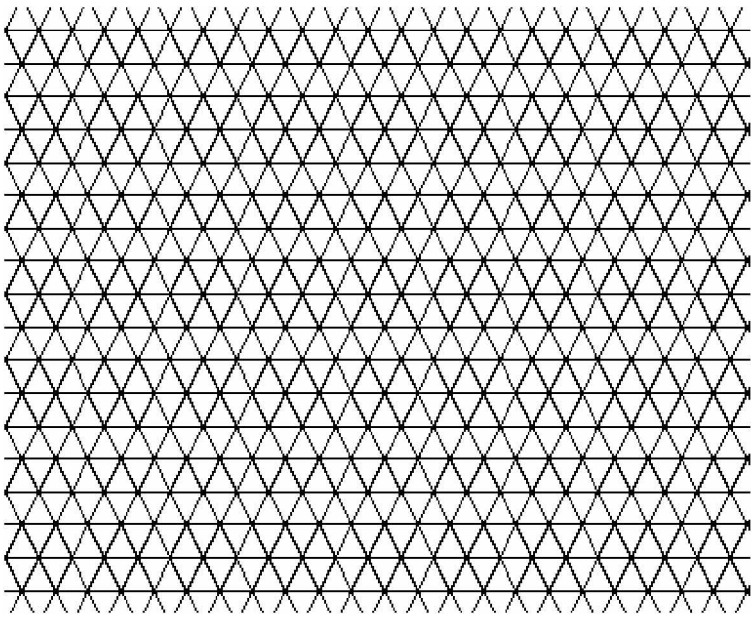

Figure 2.16: Mesh 1

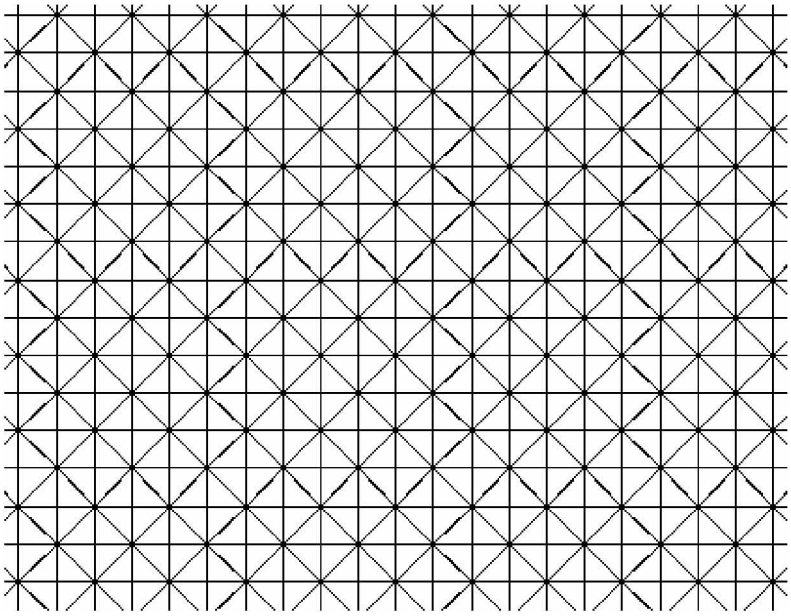

Figure 2.17: Mesh 2

Another python script had to be written to map properties generated from HYDRO_GEN on a finite difference grid to the grids presented above. For each of the nodes, a finite-difference grid block is found and its properties are mapped to the node.

2.8 Simulation Setup

Different parameters and their influence on simulation results and polymer flooding performance have been studied. This section gives an overview of these parameters as well as the detailed input parameters.

Investigated parameters are:

1. Uncertainty of different realizations
2. Influence of viscosity ratio on recovery
3. Influence of Brooks-Corey-Parameter
4. Influence of permeability heterogeneity/variance

5. Influence of different grid configurations

6. Influence of numerical method of simulator (FEM [CSP] vs. FD [CMG])

7. (Slug Design of a Polymer Flood Project / Economic Analysis)

The workflow is illustrated in figure 2.18. Rounded rectangles represent programs written by the author, normal rectangles represent external programs. HYDRO_GEN creates stochastic permeabilities. Hydrogen2CMG.py reads the permeability field data and prepares it for use with CMG's IMEX simulator.

MeshGenerator.py calculates coordinates for nodes of the finite-element mesh. PropertyMapper.py assigns the permeability values from HYDRO_GEN to the nodes, which are later meshed by triangle and finally used for simulation with CSP.

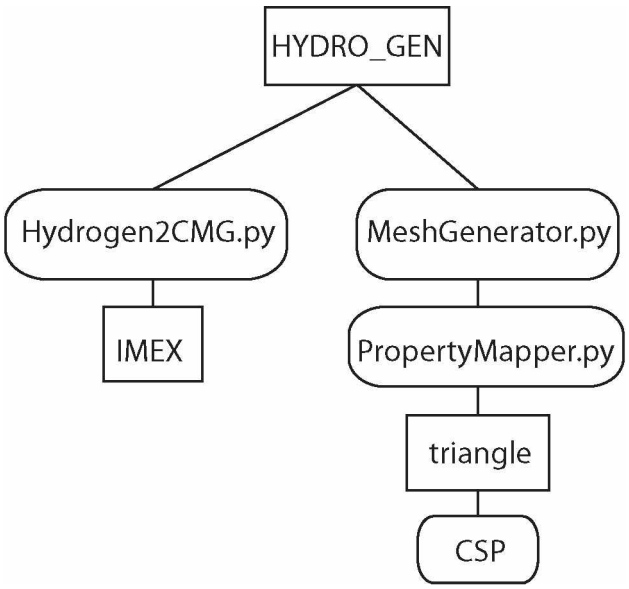

Figure 2.18: Workflow

A stochastic permeability model with five independent realizations was generated using HYDRO_GEN. The factors c and β were set to 0.1 to get a very realizations. Permeability was assumed to be distributed log-normally[Kelkar and Gupta, 1991]. The mean log-permeability was set to -12.5. The permeability field realizations and their statistics

can be seen in the next figures:

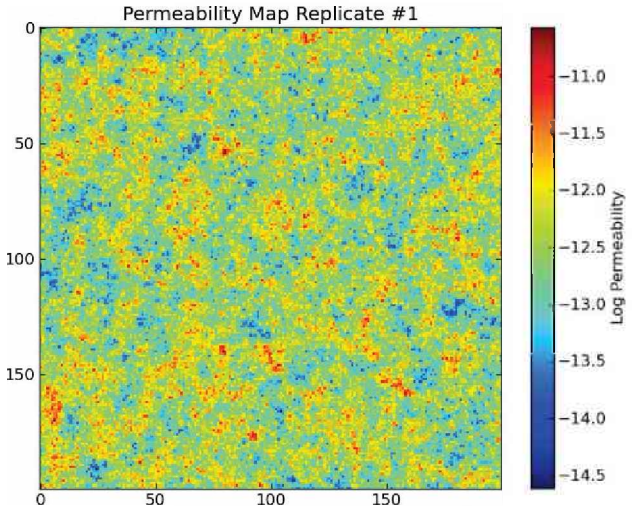

Figure 2.19: Permeability Realization #1

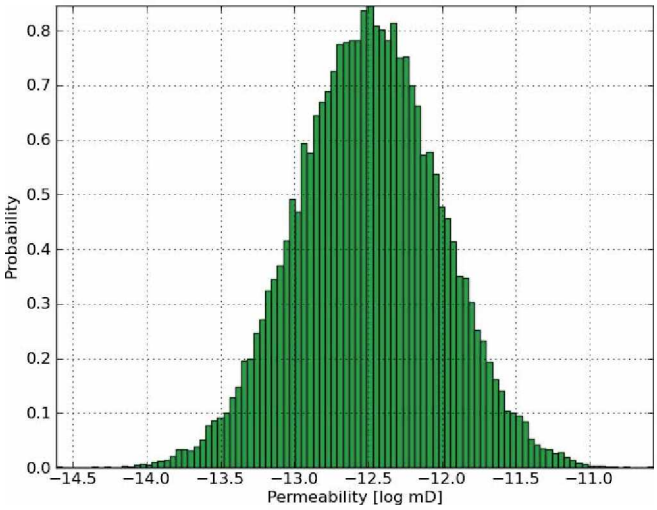

Figure 2.20: Statistics of Realization #1

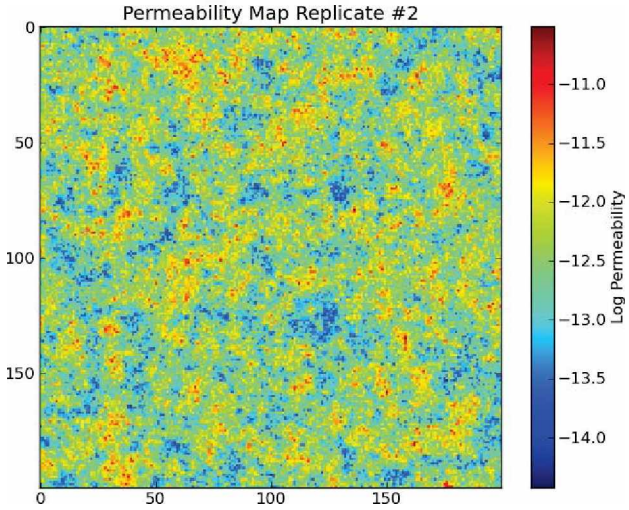

Figure 2.21: Permeability Realization #2

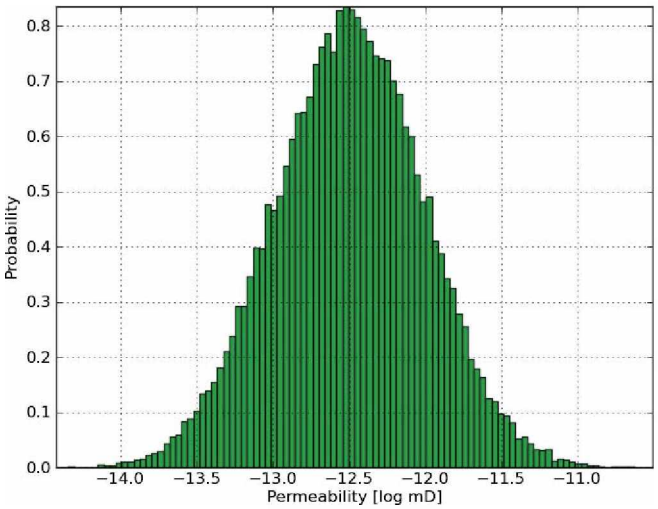

Figure 2.22: Statistics of Realization #2

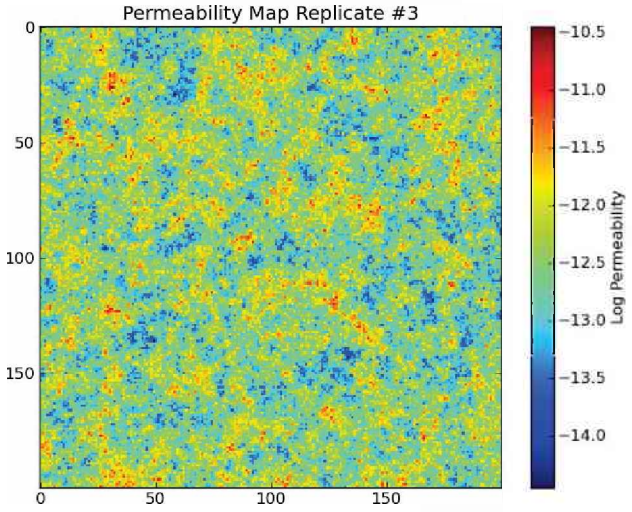

Figure 2.23: Permeability Realization #3

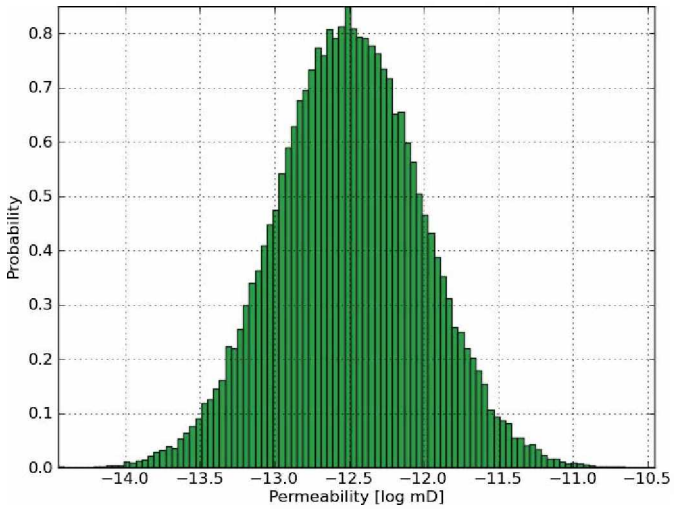

Figure 2.24: Statistics of Realization #3

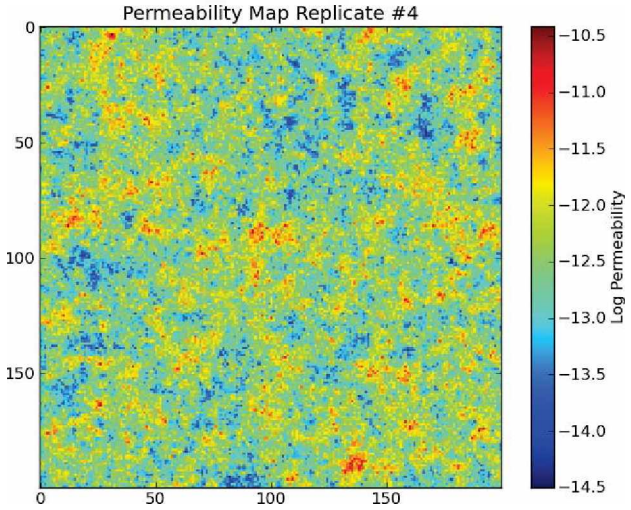

Figure 2.25: Permeability Realization #4

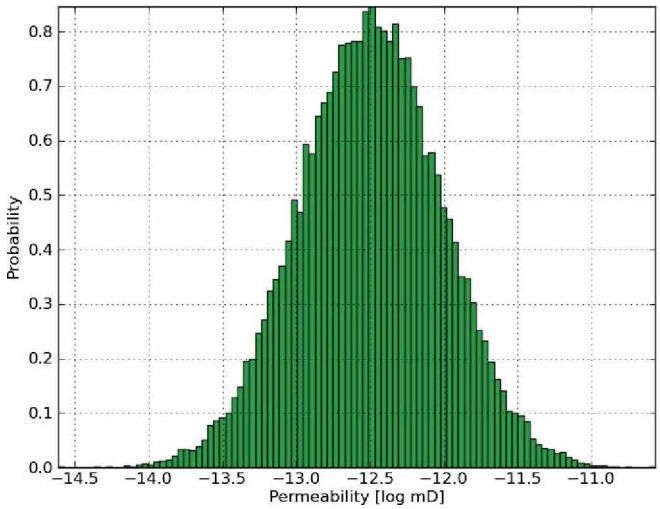

Figure 2.26: Statistics of Realization #4

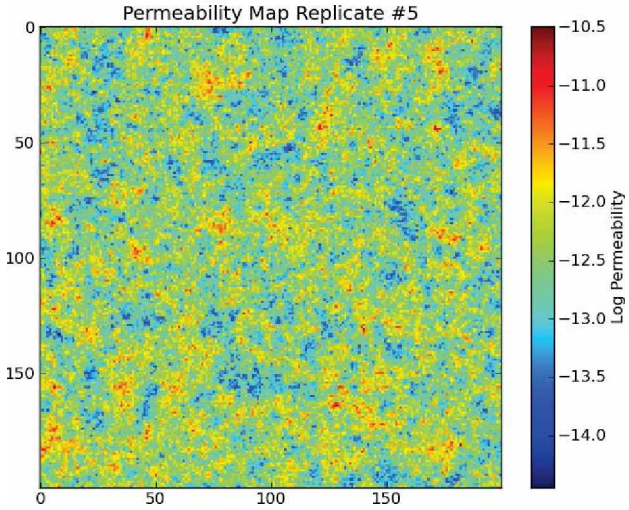

Figure 2.27: Permeability Realization #5

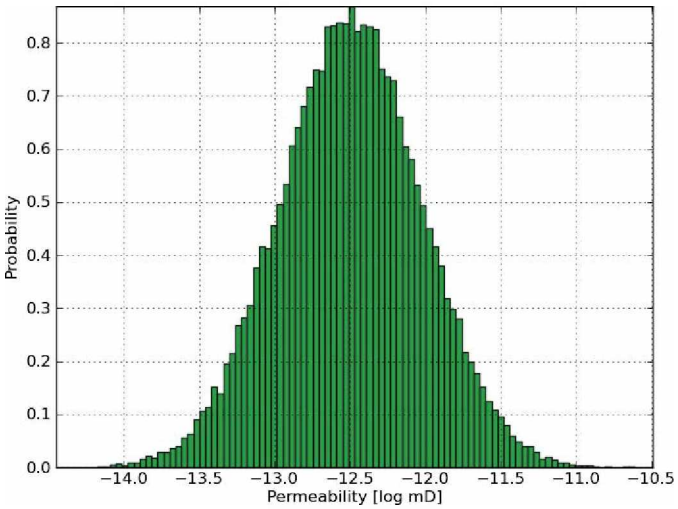

Figure 2.28: Statistics of Realization #5

The realizations are then simulated and evaluated in respect to time of water breakthrough and recovery at water breakthrough. After that, the influence of the viscosity ratio has been investigated for viscosity ratios of 1, 10, 25 and 50.

The influence of the Brooks-Corey-Parameter has been investigated by varying between 1 and 3.

To study the influence of heterogeneity, the standard deviation of permeability was decreased while maintaining the mean constant[Moissis et al., 1988]. Each node was assigned a new permeability value based on the formula:

$$k_{new} = k_{old} - 0.5(k_{old} - \bar{k}) \tag{2.68}$$

Figure 2.29 shows a histogram plot of the new permeability field:

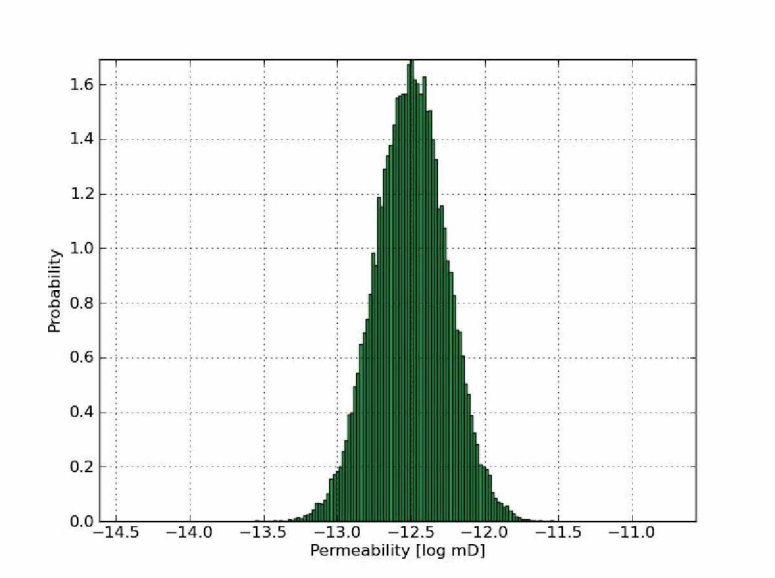

Figure 2.29: Modified Statistics of Realization #1

To study the influence of different grid configurations, two types of grids shown in figures 2.16 and 2.17. After that, an identical simulation case based on replicate 1 with a viscosity ratio of 50 was set up on a commercial simulator based on Finite Differences (CMG) and on a Finite-Element/Finite-Volume simulator (CSP).

Because a continuous polymer flood may be uneconomical due to the amount of injected polymers, a certain slug size of injected polymers can be followed by drive water or a number of slugs decreasing in concentration and therefore viscosity. Jewett and Schurz

compared different polymer injection projects and found that slug sizes from 7 to 33 percent pore volume yielded the best results[Jewett and Schurz, 1970]. I have performed simulations with different slug sizes. The results are compared with the waterflood results as well as with a pure polymer flood simulation. A short economic analysis is performed..

3 Results

3.1 Uncertainty of Different Realizations

Simulations were run up to 500 days. The first realization with breakthrough was realization number 1 with breakthrough after 390 days. Realization number 5 had a breakthrough time of 445 days followed by realization number 4 with breakthrough after 495 days.

Figures 3.1 to 3.5 show the oil saturation at breakthrough time of realization 1.

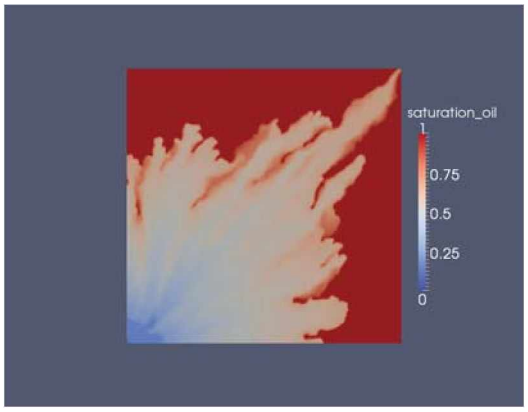

Figure 3.1: Oil Saturation Realization 1

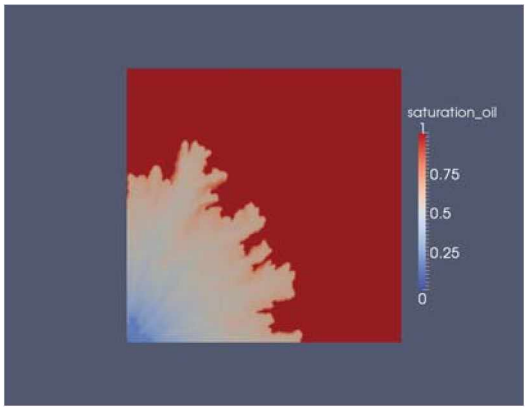

Figure 3.2: Oil Saturation Realization 2

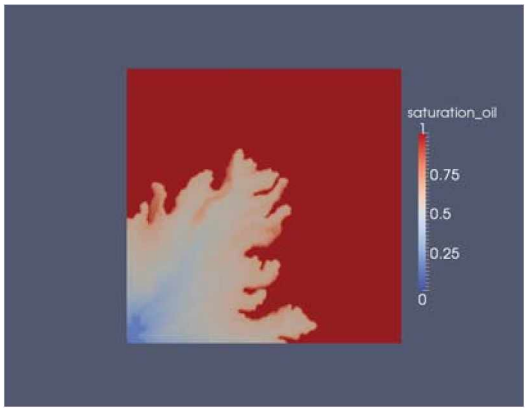

Figure 3.3: Oil Saturation Realization 3

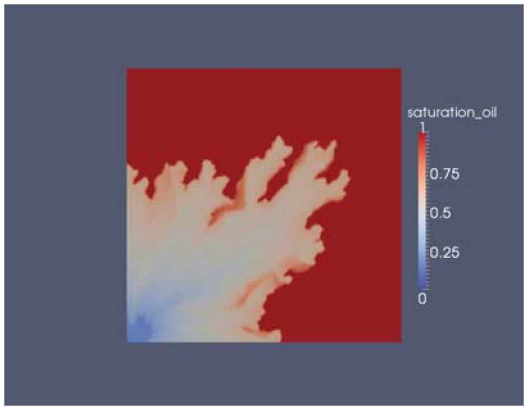

Figure 3.4: Oil Saturation Realization 4

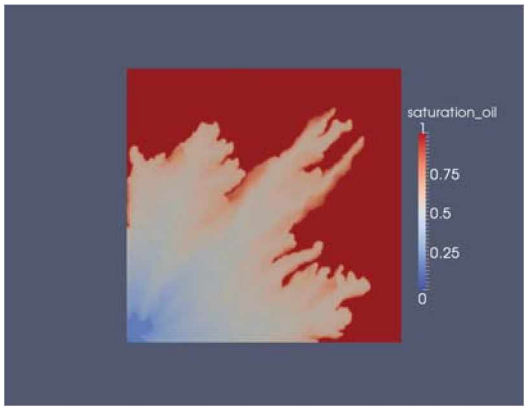

Figure 3.5: Oil Saturation Realization 5

The uncertainty span of oil recovery after 505 days is +/-14.88%.

Total volume and integrated water saturation values of realizations 1 to 5 are depicted in table 3.1.

Realization	#1	# 2	# 3	# 4	# 5
Integrated Water Saturation [m^3]	2245.77	1427.78	1424.57	1743.67	2108.17
Total Volume [m^3]	6724.98	6752.63	6742.59	6759.28	6713.67

Table 3.1: Volume Values for Different Realizations

3.2 Influence of Viscosity Ratio

The viscosity ratio was set from 1 (same viscosity for oil and polymer solution [50 cP]) up to 50 (oil 50 times more viscous than polymer solution/water). The experiments have been performed with realization 1 and with fixed injection and production pressures. A viscosity ratio of 50 lead to a breakthrough time of 390 days and a viscosity ratio of 25 to a breakthrough time of 480 days.

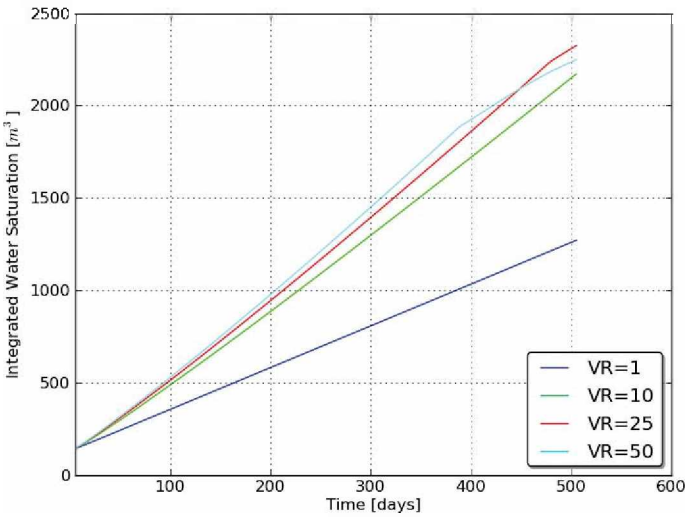

Figure 3.6: Different Viscosity Ratios

Figures 3.7 to 3.10 illustrate the oil saturation at 505 days for the different viscosity ratios.

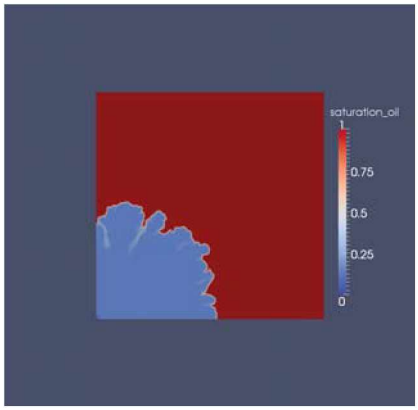

Figure 3.7: Oil Saturation for a Viscosity Ratio of 1

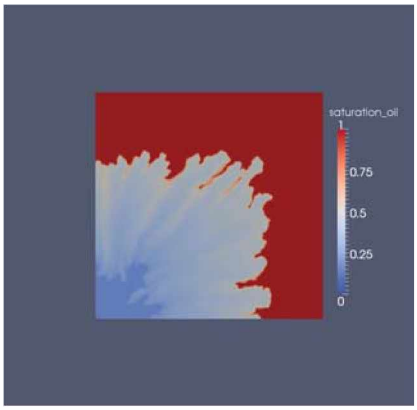

Figure 3.8: Oil Saturation for a Viscosity Ratio of 10

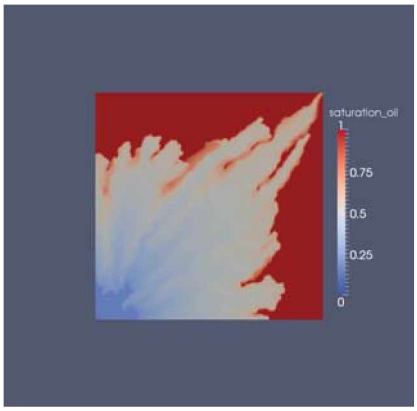

Figure 3.9: Oil Saturation for a Viscosity Ratio of 25

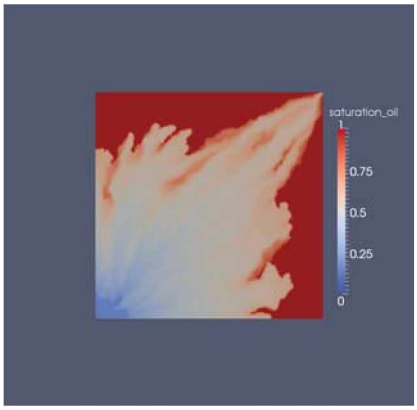

Figure 3.10: Oil Saturation for a Viscosity Ratio of 50

Viscosity Ratio	1	10	25	50
Integrated Water Saturation [m^3]	1269.69	2168.19	2321.45	2245.77

Table 3.2: Volume Values for Different Viscosity Ratios

3.3 Influence of Brooks-Corey-Parameter

The Brooks-Corey parameter was varied between typical values of 1 and 3. The influence on water saturation versus time is displayed in figure 3.3. Breakthrough time for a Brooks-Corey parameter of 1 was 475 days, 405 days for a value of 2 and 380 days for a value of 3.

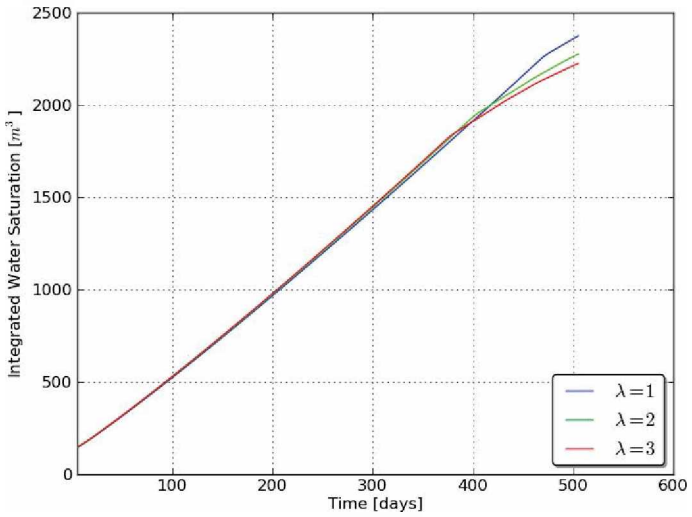

Figure 3.11: Water Saturation for Different Brooks Corey Parameters

Brooks-Corey Parameter	1	2	3
Integrated Water Saturation [m^3]	2373.92	2275.76	2225.31

Table 3.3: Volume Values for Different Brooks-Corey Parameters

3.4 Influence of Permeability Heterogeneity/Variance

Breakthrough times for the more heterogeneous case was 390 days and 440 days for the case with less permeability standard deviation. Integrated water saturation was 1886 $m^3$for the heterogeneous and 1796.8 m^3 for the homogeneous case.

Figure 3.12 shows viscous fingering in the heterogeneous case (left) and in the more homogeneous case (right).

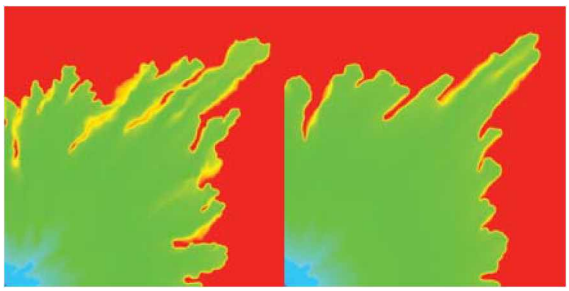

Figure 3.12: Finger Patterns of Heterogeneous versus Homogeneous Case

3.5 Influence of Different Grid Configurations

With the grid shown in figure 2.16, breakthrough occured after 390 days as opposed to 400 days with grid 2.17. Oil saturations at breakthrough are depicted in figure 3.15 and 3.13. Integrated water saturation was 1888 m^3 for mesh 1 at breakthrough and 2059.9 m^3 for mesh 2.

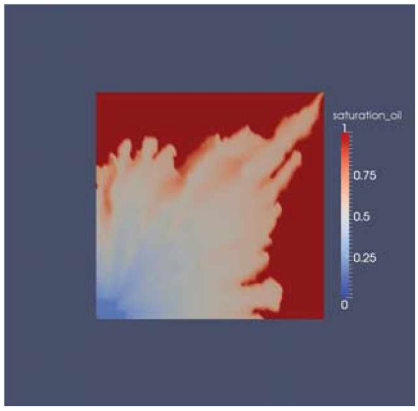

Figure 3.13: Oil Saturation at Breakthrough (Triangle Mesh)

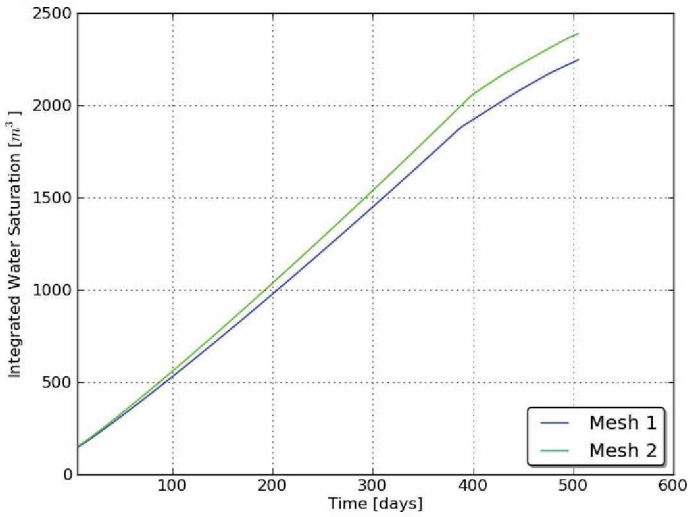

Figure 3.14: Water Saturation for Different Meshes

3.6 Influence of Numerical Method (FEM vs. FD)

Water breakthrough occured after 390 days in the CSP simulation and after 283 days in CMG. Integrated water saturation at breakthrough was 1188 m^3 in the CSP model and 1498.4 m^3 in the CMG model. Figures 3.15 and 3.16 show oil saturation at breakthrough in both simulation models. After 505 days, integrated water saturation in the CSP model

was 2245.8 m^3 and 2324 m^3 in the CMG model.

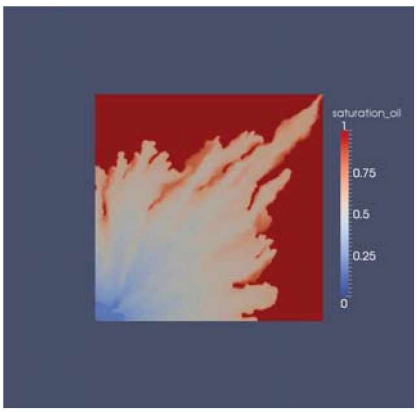

Figure 3.15: Oil Saturation at Breakthrough (CSP)

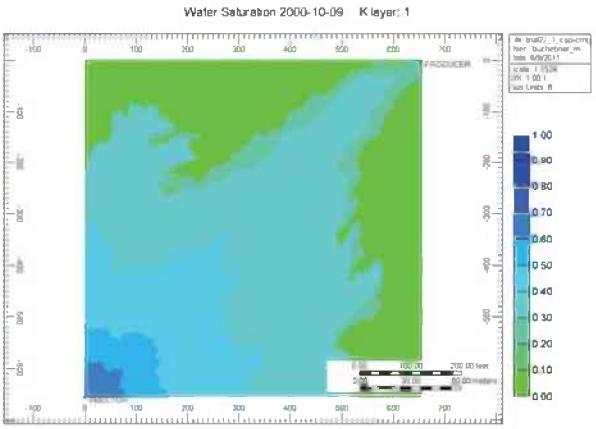

Figure 3.16: Oil Saturation at Breakthrough (CMG)

Figures 3.17 and 3.18 show the sweep pattern in early time, figures 3.19 and 3.20 at a later stage.

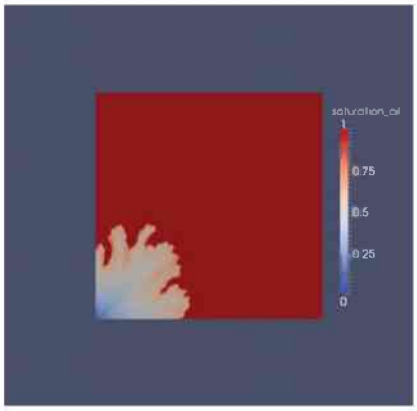

Figure 3.17: Oil Saturation at 100 days (CSP)

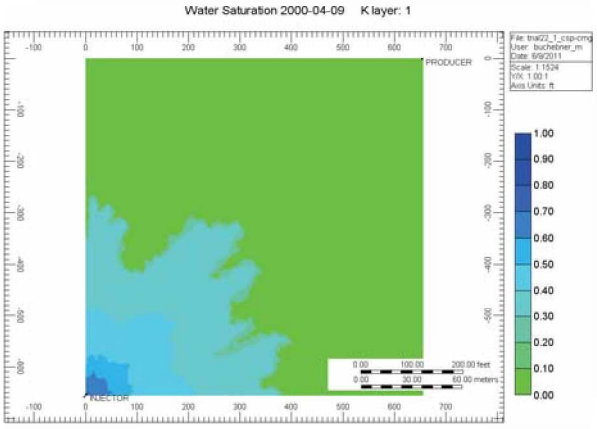

Figure 3.18: Oil Saturation at 100 days (CMG)

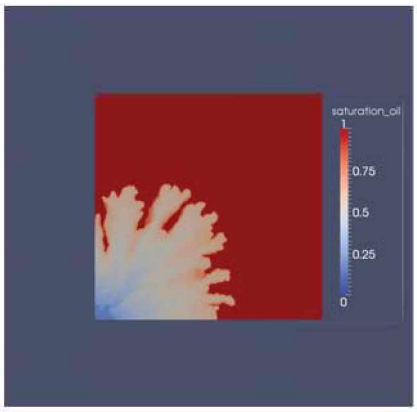

Figure 3.19: Oil Saturation at 200 days (CSP)

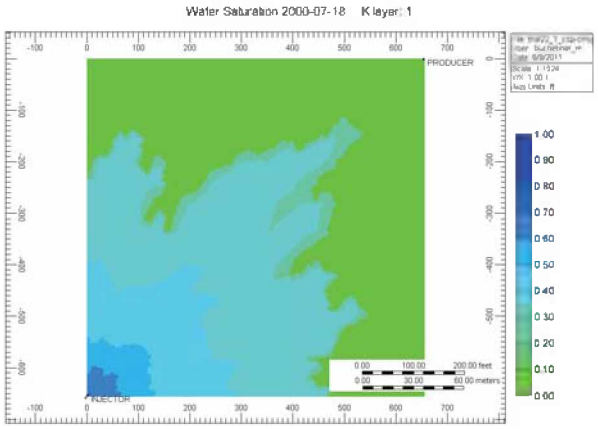

Figure 3.20: Oil Saturation at 200 days (CMG)

4 Discussion

4.1 Uncertainty of Different Realizations

Results show that permeability distribution plays a big role on recovery efficiency even if the statistical distribution and the pore volume (calculated from permeability) are the same. Realization 1 (figure 3.1) shows a finger that grows along the path between injector and producer and some other quite long fingers, leading to early breakthrough. Realization 2 (figure 3.2) shows relative stable displacement. Due to permeability disturbances, smaller fingers grow in various directions. Realization 3 (figure 3.3) has a broad finger with an orientation that is a bit off from the path to the producer and a major finger pointing to the east. Realization 4 (figure 3.4) shows to fingers in the direction of the producer and a few minor fingers in other directions. Realization 5 (figure 3.5) displays similar behaviour like realization 1, with major fingers in the direction of the producer.

4.2 Influence of Viscosity Ratio on Recovery

Figure 3.6 shows that higher polymer solution viscosity leads to later breakthrough, however, due to the higher viscosity and the constant pressure differential, less injection rate is achieved. Figures 3.7 to 3.10 show that with increasing viscosity ratio, the size of the fingers and the magnitude of instability increase.

The fingers pointing to the producer grow fastest in time.

4.3 Influence of Brooks-Corey-Parameter

Results show that the lower the Brooks-Corey parameter is, the higher recovery can be established. The difference gets smaller and smaller with increasing Brooks-Corey parameter. This parameter is inverse proportional to grain uniformity of the porous medium. A uniform grain distribution is indicative of a better recovery.

4.4 Influence of Permeability Heterogeneity/Variance

Results establish that permeability heterogeneity plays a big role in polymer flooding. The more heterogeneous the field is, the earlier breakthrough occurs since permeability variations may trigger viscous fingering. Fingers in the more heterogeneous case are not as smooth and regular as in the more homogeneous case which can be seen in figure 3.12.

4.5 Influence of Different Grid Configurations

Figure 3.13 and 3.15 show that the equiangular grid resolves small displacement instabilities much better. Small, thin fingers tend to merge in the grid with less degrees of freedom. The less degrees of freedom a mesh provides, the more smearing of discontinuities occurs.

4.6 Influence of Numerical Method (FEM vs. FD)

As the results show, the simulation results are quite different in the two simulations. Breakthrough time is almost 100 days different. The difference in integrated water saturation tends to get smaller over time.

The images show that the finite-element based simulator CSP outputs much finer structured fingers whereas the finite-difference based simulator CMG tends to "smear" them. The reason for that might the higher degree of freedom available in the Finite

Element Method.

5 Conclusion

- Stochastic properties of permeability fields play a big role. Different realizations may yield a big difference in terms of breakthrough time/recovery efficiency.
- High permeability heterogeneities trigger viscous fingers.
- The higher the viscosity ratio, the higher the magnitude of viscous fingers.
- Viscous fingers grow fastest in the direction of flow.
- The lower the viscosity ratio, the stabler the flow pattern.
- If the viscosity ratio is low, fingers tend to spread out in directions apart from the main flow direction as well.
- The higher the viscosity ratio, the earlier the breakthrough of water arrives.
- The Brooks-Corey parameter is indirectly proportional to the amount of oil recovered.
- A comparison of a Finite-Element/Finite-Volume based simulator (CSP) with a Finite-Difference based simulator (CMG) shows that the Finite-Element based approach is much more accurate in resolution of fingering phenomena.
- Higher standard deviation or heterogeneity of permeability leads to viscous fingering and earlier breakthrough.

- An equiangular mesh yields a better resolution and more accurate calculation of displacement.

Bibliography

[AlSofi and Blunt, 2009] AlSofi, A. and Blunt, M. (2009). Streamline-based simulation of non-newtonian polymer flooding. *SPEJ*, (SPE 123971).

[Bang and Caudle, 1984] Bang, H. W. and Caudle, B. H. (1984). Modeling of a micellar/polymer process. *SPEJ*, (SPE 9009).

[Bellin and Rubin, 1996] Bellin, A. and Rubin, Y. (1996). Hydrogen - a new random field generator for correlated properties. *Stochastic Hydrology and Hydraulics.*

[Bilgesu and Ertekin, 1985] Bilgesu, H. and Ertekin, T. (1985). Development of a multipurpose numerical model. *SPEJ*, (SPE 14521).

[Bondor et al., 1972] Bondor, P. L., Hirasaki, G. J., and Tham, M. (1972). Mathematical simulation of polymer flooding in complex reservoirs. *SPEJ*, (SPE 3524).

[Buckley and Leverett, 1942] Buckley, S. and Leverett, M. (1942). Mechanism of fluid displacements in sands. *Transactions of the AIME*, 146:107–116.

[Burri, 2008] Burri, P. (2008). World oil and gas resources: status and outlook - a rational attempt at an emotional issue. *Bulletin angewandte Geologie*, 13/1:3–26.

[Carcoana, 1992] Carcoana, A. (1992). *Applied Enhanced Oil Recovery.* Prentice Hall.

[Chen and Ma, 2006] Chen, H. and Ma (2006). *Computational Methods for Multiphase Flow in Porous Media.* SIAM.

[Christie, 1989] Christie, M. (1989). High-resolution simulation of unstable flows in porous media. *SPEJ*, (SPE 16005).

[Collins, 1961] Collins, R. E. (1961). *Flow of Fluids through Porous Materials.* PennWell Publishing Co.

[Cressie, 1993] Cressie (1993). *Statistics for Spatial Data.* Wiley Interscience.

[Dogru and Yamamoto, 1984] Dogru, A. and Yamamoto, R. (1984). Numerical simulation of micellar polymer field processes. *SPEJ*, (SPE 13121).

[Donaldson et al., 1989] Donaldson, E. C., Chilingarian, G. V., and Yen, T. F. (1989). *Enhanced Oil Recovery II - Processes and Operations.* Elsevier.

[Graue, 1968] Graue, D. (1968). A prediction method for reservoir flooding with fluids of reduced mobility. *SPEJ*, (SPE 2257).

[Green and Willhite, 1998] Green, D. W. and Willhite, G. P. (1998). *Enhanced Oil Recovery.* SPE Textbook Series Volume 6. Society of Petroleum Engineers.

[Helmig, 1997] Helmig, R. (1997). *Multiphase Fow and Transport Processes in the Subsurface.* Springer.

[Jewett and Schurz, 1970] Jewett, R. and Schurz, G. (1970). Polymer flooding - a current appraisal. *Journal of Petroleum Technology*, (SPE 2545).

[John et al., 2005] John, A., Han, C., Delshad, M., Pope, G., and Sepehrnoori, K. (2005). A new generation chemical-flooding simulator. *SPEJ*, (SPE 89436).

[Jones et al., 1984] Jones, R., Pope, G., Ford, H., and Lake, L. (1984). A predictive model for water and polymer flooding. *SPEJ*, (SPE 12653).

[Kaminsky et al., 2007] Kaminsky, R., Wattenbarger, R., Szafranski, R., and Coutee, A. (2007). Guidelines for polymer flooding evaluation and development. *IPTC*, (IPTC 11200).

[Kelkar and Gupta, 1991] Kelkar and Gupta (1991). A numerical study of viscous instabilities: Effect of controlling parameters and scaling considerations. *SPEJ*, 18094.

[Kolodziej, 1988] Kolodziej, E. (1988). Transport mechanisms of xanthan biopolymer solutions in porous media. *SPEJ*, (SPE 18090).

[Littmann, 1988] Littmann, W. (1988). *Polymer Flooding*, volume 24 of *Developments in Petroleum Science*. Elsevier.

[Lutchmansingh, 1987] Lutchmansingh, P. M. (1987). *Development and Application of a Highly Implicit, Multi Dimensional Polymer Injection Simulator*. PhD thesis, Pennsylvania State University.

[Maitin et al., 1988] Maitin, B., Daboul, B., and Sohn, W. (1988). Numerical simulation for planning and evaluation of polymer flood process: A field performance analysis. *SPEJ*, (SPE 17631).

[Matthaei, 2008] Matthaei (2008). Reservoir simulation lecture notes.

[Matthäi et al., 2004] Matthäi, S., Geiger, S., and Roberts, S. (2004). *The Complex Systems Platform CSP3D3.0: User's Guide.*

[Moissis et al., 1988] Moissis, D. E., Miller, C. A., and Wheeler, M. F. (1988). A parametric study of viscous fingering in miscible displacement by numerical simulation. *ACM.*

[Patton et al., 1970] Patton, J., Coats, K., and Colegrove, G. (1970). Prediction of polymer flood performance. *SPEJ*, (SPE 2546).

[Shewchuk, 2005] Shewchuk, J. R. (2005).

[Shiyi et al., 1995] Shiyi, Y., Puhua, Y., Zhongqiu, D., and Kuiyou, S. (1995). Numerical simulation of alkali/surfactant/polymer flooding. *SPEJ*, (SPE 29904).

[Slater and Farouq-Ali, 1970] Slater, G. E. and Farouq-Ali, S. (1970). Two-dimensional polymer flood simulation. *SPEJ*, (SPE 7034).

[Steinbuechel, 2003] Steinbuechel, A., editor (2003). *Biopolymers.* Wiley-VCH.

[Taber et al., 1997] Taber, J., Martin, F., and Seright, R. (1997). Eor screening criteria revisited - part 1: Introduction to screening criteria and enhanced recovery field projects. *SPEJ*, (SPE 35385).

[Todd and Chase, 1979] Todd, M. R. and Chase, C. A. (1979). A numerical simulator for predicting chemical flood performance. *SPEJ*, (SPE 7689).

[Verma et al., 2009] Verma, S., Adibhatla, B., Kaminsky, R., Wattenbarger, C., and Davidson, J. (2009). Modeling polymer flood in an unstructured grid simulator. *SPEJ*, (SPE 118985).

[Wackernagel, 1995] Wackernagel (1995). *Multivariate Geostatistics.* Springer.

[Willhite, 1986] Willhite, G. P. (1986). *Waterflooding.* SPE.

[Zeito, 1968] Zeito, G. (1968). Three dimensional numerical simulation of polymer flooding in homogeneous and heterogeneous systems. *SPEJ*, (SPE 2186).